

Hybrid computational analysis of fractional optical soliton structures in a dispersive Schrödinger model with applications in nonlinear optics

Mati ur Rahman, Sonia Akram, and Laila A. AL-Essa

Citation: Chin. Phys. B, 2026, 35 (**7**): 070503. DOI: 10.1088/1674-1056/ae5808
http://cpb.iphy.ac.cn; http://iopscience.iop.org/cpb

What follows is a list of articles you may be interested in

Periodic lump, soliton, and some mixed solutions of the (2+1)-dimensional generalized coupled nonlinear Schrödinger equations

Xiao-Min Wang(王晓敏), Ji Li(李吉), and Xiao-Xiao Hu(胡霄骁)
Chin. Phys. B, 2025, 34 (**11**): 110502. DOI: 10.1088/1674-1056/ae1019

Effective regulation of the interaction process among three optical solitons

Houhui Yi(伊厚会), Xiaofeng Li(李晓凤), Junling Zhang(张俊玲), Xin Zhang(张鑫), and Guoli Ma(马国利)
Chin. Phys. B, 2024, 33 (**10**): 100502. DOI: 10.1088/1674-1056/ad6b87

High-order effect on the transmission of two optical solitons

Houhui Yi(伊厚会), Yanli Yao(姚延立), Xin Zhang(张鑫), and Guoli Ma(马国利)
Chin. Phys. B, 2023, 32 (**10**): 100509. DOI: 10.1088/1674-1056/aceeec

Influence of the initial parameters on soliton interaction in nonlinear optical systems

Xinyi Zhang(张昕仪) and Ye Wu(吴晔)
Chin. Phys. B, 2023, 32 (**7**): 070505. DOI: 10.1088/1674-1056/ace1da

All-optical switches based on three-soliton inelastic interaction and its application in optical communication systems

Shubin Wang(王树斌), Xin Zhang(张鑫), Guoli Ma(马国利), and Daiyin Zhu(朱岱寅)
Chin. Phys. B, 2023, 32 (**3**): 030506. DOI: 10.1088/1674-1056/acad6c

---

Hybrid computational analysis of fractional optical soliton structures in a dispersive Schrödinger model with applications in nonlinear optics

Mati ur Rahman[1], Sonia Akram [2], and Laila A. AL-Essa[3,†]

[1] *Department of Mathematics and Statistics, College of Sciences, Imam Mohammad Ibn Saud Islamic University (IMSIU), Riyadh, Saudi Arabia*
[2] *Department of Mathematics, Faculty of Science, University of Gujrat, Gujrat-50700, Pakistan*
[3] *Department of Mathematical Sciences, College of Science, Princess Nourah bint Abdulrahman University, P.O. Box 84428, Riyadh 11671, Saudi Arabia*

(Received 8 December 2025; revised manuscript received 7 March 2026; accepted manuscript online 27 March 2026)

The present study aims to integrate and explore optical solitary wave solutions within the framework of the high-order fractional dispersive extended nonlinear Schrödinger model (FDENLSM), a refined mathematical formulation with wide-ranging applications in nonlinear physics, optical communications, and field theory. By utilizing three contemporary computational approaches, namely, the modified Sardar sub-equation method, the new Kudryashov approach, and the improved F-expansion method, we obtain and systematically analyze a rich spectrum of optical soliton structures, including dark, singular, bright, periodic, exponential, rational, and composite forms. Furthermore, distinct wave patterns such as W-shaped, bell-shaped, peakon, and mixed trigonometric–hyperbolic solitons are also investigated. The study extends to the examination of modulation instability and gain spectra of the FDENLSM, providing deeper insight into the system's nonlinear characteristics. To vividly signify the obtained results, contour and density maps are presented in both two- and three-dimensional perspectives. The outcomes of this research contribute significantly to the understanding of complex nonlinear propagation phenomena, offering valuable analytical tools for researchers working in plasma dynamics, fiber optics, and related nonlinear systems.

Keywords: FDENLSM, truncated M-fractional derivative, analytical techniques, optical solitons, modulation instability

PACS: 05.45.Yv, 04.30.Nk, 02.30.Jr, 04.20.Jb

DOI: 10.1088/1674-1056/ae5808 **CSTR:** 32038.14.CPB.ae5808

1. Introduction

The scientific description of complex manifestations across many systematic fields is made possible by nonlinear partial differential equations (NLPDEs), which are essential for providing careful insight into the intricately evolving characteristics of natural systems.[1] In contrast, NLPDEs suggest solutions that are opposite to those of their linear counterparts. These NLPDEs defy direct superposition rules, leading to an increasingly complex range of dynamics, including bifurcations, chaos, and intricate spatiotemporal patterns.[2] Through the cooperation of nonlinear components, these models demonstrate a variety of physical phenomena, such as fluid dynamics, heat transfer, and optics, where the nonlinearity of fundamental physical principles is manifested. The analysis and study of nonlinear partial differential equations deepen our theoretical understanding of complicated structures and reveal crucial insights into their evolving behavior. Such analysis is very important for the interpretation, prediction, and monitoring of different real-world phenomena.[3,4] Numerous phenomena, such as optics, nonlinear fibre optics, plasma physics, engineering, and physical effects in fluid dynamics, can be effectively characterized by NLPDEs.[5–7] The nonlinear Schrödinger equation (NLSE) is a fundamental tool in many scientific fields and technical applications. In communication systems, the NLSE is essential for simulating the propagation of optical pulses through optical fibres. Engineers can forecast and improve the performance of optical communication systems, including pulse shaping, nonlinear effects, and signal dispersion, by solving the NLSE. The NLSE plays an important role in many scientific and engineering domains, such as quantum mechanics, optics, laser technology, ultracold physics, and biology.[8,9] Numerous scientific and technical fields are advanced by its solutions, which also provide valuable insights into the behavior of complex systems governed by nonlinear wave equations.

An area of mathematics known as fractional calculus (FC), which deals with derivatives and integrals of non-integer order, is also very important in a variety of scientific fields and engineering applications. The behaviors of many natural systems and processes are too complex for traditional integer-order calculus to accurately represent. A strong mathematical

†Corresponding author. E-mail: Laalessa@pnu.edu.sa

© 2026 Chinese Physical Society and IOP Publishing Ltd. All rights, including for text and data mining, AI training, and similar technologies, are reserved.

foundation for simulating intricate events with memory, long-range interactions, and non-locality is offered by FC. Non-local effects are captured by FC, meaning that a system's current state depends on its historical performance over a span of time or space. Numerous physical systems, including fractional diffusion processes, fractional Brownian motion, and porous medium flow, exhibit this characteristic. Many dynamical systems show complex behaviors involving long-range interactions and memory effects. Its applications span from basic research to useful engineering solutions, pushing the boundaries of industry, science, and technology.[10]

In many areas of physics, such as condensed matter physics, Bose-Einstein condensates, plasma physics, and nonlinear optics, the NLSE is a fundamental partial differential equation.[11] The NLSE is often used to simulate how optical pulses propagate through nonlinear optical fibers. It helps to understand phenomena such as self-phase modulation, four-wave mixing, and supercontinuum generation. Numerous extensions and generalizations of the NLSE have been developed to incorporate additional effects such as dissipation, higher-order nonlinearities, and external potentials. These extensions allow a more comprehensive description of physical systems and enable the exploration of new phenomena. In the context of the high-order NLSE, consideration of third-order dispersion (TOD) and fourth-order dispersion (FOD) terms becomes significant due to their impact on the dynamics of optical pulses in dispersive media.[12] TOD and FOD terms introduce additional complexities into the dispersion properties of the medium. They can cause temporal spreading and distortion of optical pulses as they propagate through the medium. The presence of higher-order dispersion terms affects the stability, propagation, and interaction of these solitons, leading to rich dynamics and novel phenomena. Consideration of third- and fourth-order dispersion terms in the high-order NLSE is essential for understanding the intricate dynamics of optical pulses in dispersive media and for designing advanced optical communication systems and nonlinear optical devices.[13] To thoroughly analyze dynamics and apply NLPDEs to practical problems, analytical solutions are significant. Many efficient techniques have been developed over time to construct analytical solutions for NLPDEs. To better understand real-world phenomena, some researchers have employed techniques such as the Khater method,[14] the Sardar sub-equation method,[15] the modified exponential function method,[16] Lie symmetry analysis,[17] the unified method,[18] the Hirota bilinear method,[19] the Heir equation method,[20] the Adomian decomposition method,[21] the Nucci reduction method,[22] and the Darboux transformation method.[23]

Despite the amount of study that has already been conducted on the high-order FDENLSM, more comprehensive investigations combining various analytical techniques are urgently needed to obtain accurate solutions.[24] For addressing a broad spectrum of nonlinear phenomena, the accuracy and diversity of these solutions are essential. By analyzing the FDENLSM using the MSSE method, the new Kudryashov methodology, and the enhanced $\mathcal{F}$-expansion method, this study seeks to bridge this knowledge gap. The primary goal of this study is to investigate the high-order FDENLSM in detail and propose practical methods for obtaining accurate and reliable solutions. Additionally, the modulation instability (MI) of the proposed model is examined; these investigations have produced a large number of isolated findings that have not been reported in earlier research.

The mathematical formulation of the high-order FDENLSM equation is given by[25,26]

$$-\frac{\wp_4}{24}D_{M,x}^{4\alpha,\beta}\Lambda-\mathrm{i}\frac{\wp_3}{6}D_{M,x}^{3\alpha,\beta}\Lambda-\frac{\wp_1}{2}D_{M,x}^{2\alpha,\beta}\Lambda+\wp_5\Lambda|\Lambda|^4+\wp_2\Lambda|\Lambda|^2+\mathrm{i}D_{M,t}^{\alpha,\beta}\Lambda=0. \tag{1}$$

The function $\Lambda=\Lambda(x,t)$ describes a temporally and spatially dependent entity that encapsulates the complex envelope of a nonlinear dispersive wave or pulse. $D_{M,x}^{\alpha,\beta}$ is the M-truncated derivative. Here, t and x denote the time and spatial propagation coordinates, respectively. The amplitude profile of the electric field is represented by the real component of Λ, while the phase profile is represented by the imaginary part. The second-order dispersion coefficient, denoted by $\wp_1$, indicates the group velocity dispersion as well as the extent to which chromatic effects cause the pulse to spread. $\wp_2$ refers to the nonlinear coefficient for the Kerr effect, which signifies the nonlinear response and self-phase modulation. $\wp_3$ is the TOD coefficient. Also, the influence of TOD on pulse propagation is determined by its magnitude. $\wp_4$ is the FOD coefficient. For the saturated nonlinear response term, the nonlinear coefficient is $\wp_5$. One can express a saturated nonlinear response of the medium as a $\Lambda|\Lambda|^4$ nonlinear term proportional to $|\Lambda|^4$. The $\Lambda|\Lambda|^2$ nonlinear term proportional to $|\Lambda|^2$ defines the model's instantaneous Kerr nonlinearity, as in the NLSE. Several academics have recently investigated the NLSE using various unconventional methods. For instance, Akram *et al.*[27] investigated the perturbed NLSE arising in optics by combining the enhanced F-expansion method with an alternative soliton solution. According to the authors,[28] the NLSE exhibits both bright and dark solitons. Using nonlinear chromatic dispersion and extracting optical soliton solutions, Mathanaranjan *et al.*[29] employed the new extended auxiliary equation approach for the NLSE. To discover solitary wave solutions, the authors in Ref. [30] employed the innovative extended unified auxiliary equation approach for the high-order NLSE.

The remainder of this article is structured as follows: Section 2 presents the characteristics of the M-fractional derivative. Section 3 provides a brief overview of the selected tech-

niques. Section 4 signifies how to apply the selected techniques to Eq. (1) and obtain soliton solutions. The MI is presented in Section 5. The physical explanations of the developed solutions are explored in Section 6. Finally, Section 7 synthesizes the conclusions.

2. The M-truncated derivative

FC is extended by the M-truncated derivative, which introduces a truncation parameter M. This parameter restricts the influence of distant historical data on the computation of the current derivative.

Definition The following is the truncated M-fractional derivative[31] of order α for a function $f:(0,\infty)\to R$

$$D_M^{\alpha,\beta}g[\varpi]=\lim_{\varepsilon\to 0}\frac{g(\varpi E_\beta(\varepsilon\varpi^{1-\alpha}))-g(\varpi)}{\varepsilon},$$
$$\varpi>0,\ \ \forall\, 0<\alpha\le 1,\ \ \beta>0, \tag{2}$$

where $E_\beta(\cdot)$ is a Mittag-Leffler function.

Theorem 1 Assume that $\alpha\in(0,1]$, $\beta>0$, and $f=f(\varpi)$ and $g=g(\varpi)$ are α-differentiable at a point $\varpi>0$. Some properties of the above-mentioned derivative are

(i) $D_M^{\alpha,\beta}(ag+bh)=aD_M^{\alpha,\beta}g+bD_M^{\alpha,\beta}h,\ \forall a,\ b\in R,$

(ii) $D_M^{\alpha,\beta}(c)=0,$ where c is a constant,

(iii) $D_M^{\alpha,\beta}(g\cdot h)=gD_M^{\alpha,\beta}(h)+hD_M^{\alpha,\beta}(g),$

(iv) $D_M^{\alpha,\beta}(\frac{g}{h})=\dfrac{hD_M^{\alpha,\beta}(g)-gD_M^{\alpha,\beta}(h)}{h^2(\varpi)}.$

Also, $D_M^{\alpha,\beta}(f(\varpi))=\frac{\varpi^{1-\alpha}}{\Gamma(\beta+1)}\frac{\mathrm{d}f}{\mathrm{d}\varpi}$, where $f(\varpi)$ refers to a differentiable function.

3. Mathematical prelimeriers of the selected methods

We explain in this section the main methodologies and steps for solving NLPDEs. Let us consider the fractional NLPDE

$$\mathcal{G}(v,\ D_{M,t}^{\alpha,\beta}v,\ D_{M,x}^{\alpha,\beta}v,\ D_{M,2t}^{\alpha,\beta}v,\ D_{M,2x}^{\alpha,\beta}v,\ \cdots)=0. \tag{3}$$

Assume the following transformation in order to obtain the ordinary differential equation corresponding to Eq. (3)

$$v(x,t)=\mathcal{V}(\xi),\ \ \text{where}\ \ \xi=\frac{\Gamma(\beta+1)}{\alpha}(x^\alpha+\vartheta t^\alpha). \tag{4}$$

Here, $\mathcal{V}(\xi)$ represents the amplitude. Substituting Eq. (4) into Eq. (3), we obtain

$$\mathcal{R}(\mathcal{V},\ \mathcal{V}',\ \mathcal{V}'',\ \cdots)=0. \tag{5}$$

3.1. The MSSE method

The MSSE method plays a significant role in mathematical modeling, scientific research, and engineering practice by offering a systematic, efficient, and versatile approach to solving equations.

Assume the trial solution of Eq. (5) as

$$\mathcal{V}(\xi)=\gamma_0+\sum_{i=1}^{n}\gamma_i\mathcal{S}(\xi)^i,\ \gamma_n\neq 0, \tag{6}$$

where $\gamma_i(i=0,1,2,\cdots,n)$ is calculated later. The value of the integer n can be determined using the balancing theory in Eq. (5). From Eq. (6), the function $\mathcal{S}(\xi)$ satisfies the following differential equation

$$(\mathcal{S}'(\xi))^2=\rho_0+\rho_1\mathcal{S}(\xi)^2+\rho_2\mathcal{S}(\xi)^4, \tag{7}$$

where $\rho_0,\ \rho_1,\ \rho_2$ are unknowns.

Following are the results of Eq. (7) along with a constant τ:

(i) If $\rho_0=0$, $\rho_1>0$ and $\rho_2\neq 0$, then

$$\mathcal{S}_1(\xi)=\pm\sqrt{-\frac{\rho_1}{\rho_2}}\,\mathrm{sech}\,(\sqrt{\rho_1}(\xi+\tau)), \tag{8}$$

$$\mathcal{S}_2(\xi)=\pm\sqrt{-\frac{\rho_1}{\rho_2}}\,\mathrm{csch}\,(\sqrt{\rho_1}(\xi+\tau)). \tag{9}$$

(ii) For constants g_1, g_2, $\rho_0=0$, $\rho_1>0$ and $\rho_2=4\times g_1\times g_2$, then

$$\mathcal{S}_3(\xi)=\pm(4g_1\sqrt{\rho_1})/\Big[\left(4g_1^2-\rho_2\right)\sinh(\sqrt{\rho_1}(\xi+\tau))+\left(4g_1^2-\rho_2\right)\cosh(\sqrt{\rho_1}(\xi+\tau))\Big]. \tag{10}$$

(iii) For constants r_1, r_2, $\rho_0=\frac{\rho_1^2}{4\rho_2}$, $\rho_1<0$ and $\rho_2>0$, then

$$\mathcal{S}_4(\xi)=\pm\sqrt{-\frac{\rho_1}{2\rho_2}}\tanh\left(\sqrt{-\frac{\rho_1}{2}}(\xi+\tau)\right), \tag{11}$$

$$\mathcal{S}_5(\xi)=\pm\sqrt{-\frac{\rho_1}{2\rho_2}}\coth\left(\sqrt{-\frac{\rho_1}{2}}(\xi+\tau)\right), \tag{12}$$

$$\mathcal{S}_6(\xi)=\pm\sqrt{-\frac{\rho_1}{2\rho_2}}\left[\tanh\left(\sqrt{-\frac{\rho_1}{2}}(\xi+\tau)\right)+\mathrm{isech}\left(\sqrt{-2\rho_1}(\xi+\tau)\right)\right], \tag{13}$$

$$\mathcal{S}_7(\xi)=\pm\sqrt{-\frac{\rho_1}{8\rho_2}}\left[\tanh\left(\sqrt{-\frac{\rho_1}{8}}(\xi+\tau)\right)+\mathrm{icoth}\left(\sqrt{-\frac{\rho_1}{8}}(\xi+\tau)\right)\right], \tag{14}$$

$$\mathcal{S}_8(\xi)=\pm\frac{\sqrt{-\frac{\rho_1}{2\rho_2}}\left[\sqrt{r_1^2+r_2^2}-r_1\cosh(\sqrt{-2\rho_1}(\xi+\tau))\right]}{r_1\sinh(\sqrt{-2\rho_1}(\xi+\tau))+r_2}, \tag{15}$$

$$\mathcal{S}_9(\xi)=\pm\frac{\sqrt{-\frac{\rho_1}{2\rho_2}}\cosh(\sqrt{-2\rho_1}(\xi+\tau))}{\sinh(\sqrt{-2\rho_1}(\xi+\tau))+s}. \tag{16}$$

(iv) If $\rho_0 = 0$, $\rho_1 < 0$ and $\rho_2 \neq 0$, then

$$\mathcal{S}_{10}(\xi) = \pm\sqrt{-\frac{\rho_1}{\rho_2}}\sec\left(\sqrt{-\rho_1}(\xi+\tau)\right), \tag{17}$$

$$\mathcal{S}_{11}(\xi) = \pm\sqrt{-\frac{\rho_1}{\rho_2}}\csc\left(\sqrt{-\rho_1}(\xi+\tau)\right). \tag{18}$$

(v) If $\rho_0 = \frac{\rho_1^2}{4\rho_2}$, $\rho_1 > 0$ and $\rho_2 > 0$ and $r_1^2 - r_2^2 > 0$, then

$$\mathcal{S}_{12}(\xi) = \pm\sqrt{-\frac{\rho_1}{2\rho_2}}\tan\left(\sqrt{\frac{\rho_1}{2}}(\xi+\tau)\right), \tag{19}$$

$$\mathcal{S}_{13}(\xi) = \pm\sqrt{-\frac{\rho_1}{2\rho_2}}\cot\left(\sqrt{\frac{\rho_1}{2}}(\xi+\tau)\right), \tag{20}$$

$$\mathcal{S}_{14}(\xi) = \pm\sqrt{-\frac{\rho_1}{2\rho_2}}\left[\tan\left(\sqrt{2\rho_1}(\xi+\tau)\right) - \sec\left(\sqrt{2\rho_1}(\xi+\tau)\right)\right], \tag{21}$$

$$\mathcal{S}_{15}(\xi) = \pm\sqrt{-\frac{\rho_1}{8\rho_2}}\left[\tan\left(\sqrt{\frac{\rho_1}{8}}(\xi+\tau)\right) - \cot\left(\sqrt{\frac{\rho_1}{8}}(\xi+\tau)\right)\right], \tag{22}$$

$$\mathcal{S}_{16}(\xi) = \pm\frac{\sqrt{-\frac{\rho_1}{2\rho_2}}\left[\sqrt{r_1^2 - r_2^2} - r_1\cos\left(\sqrt{2\rho_1}(\xi+\tau)\right)\right]}{r_1\sin\left(\sqrt{2\rho_1}(\xi+\tau)\right) + r_2}, \tag{23}$$

$$\mathcal{S}_{17}(\xi) = \pm\frac{\sqrt{-\frac{\rho_1}{2\rho_2}}\cos\left(\sqrt{2\rho_1}(\xi+\tau)\right)}{\sin\left(\sqrt{2\rho_1}(\xi+\tau)\right) - 1}. \tag{24}$$

(vi) If $\rho_0 = 0$, $\rho_1 > 0$, then

$$\mathcal{S}_{18}(\xi) = \pm\frac{4\rho_1 \mathrm{e}^{\sqrt{\rho_1}(\xi+\tau)}}{\mathrm{e}^{2\sqrt{\rho_1}(\xi+\tau)} - 4\rho_1\rho_2}, \tag{25}$$

$$\mathcal{S}_{19}(\xi) = \pm\frac{4\rho_1 \mathrm{e}^{\sqrt{\rho_1}(\xi+\tau)}}{1 - 4\rho_1\rho_2 \mathrm{e}^{2\sqrt{\rho_1}(\xi+\tau)}}. \tag{26}$$

(vii) If $\rho_0 = 0$ and $\rho_1 = 0$ and $\rho_2 > 0$, then

$$\mathcal{S}_{20}(\xi) = \pm\frac{1}{\sqrt{\rho_2}(\xi+\tau)}, \tag{27}$$

$$\mathcal{S}_{21}(\xi) = \pm\frac{\mathrm{i}}{\sqrt{\rho_2}(\xi+\tau)}. \tag{28}$$

Substituting Eqs. (6) and (7) into Eq. (5), and collecting the coefficients of each power of $\mathcal{S}(\xi)$, we obtain a system of algebraic equations with unknown variables. By setting these coefficients to zero and solving the resulting system, the unknown parameters can be determined. Finally, the exact solutions of Eq. (3) can be obtained.

3.2. The new Kudryashov scheme

A quick glance at the new Kudryashov method is described as follows:

We assume the trial solution of Eq. (5) as

$$v(\xi) = \sum_{i=0}^{N} \vartheta_i \mathcal{R}(\xi)^i, \tag{29}$$

where ϑ_i, $0 \leq i \leq N$, represent unknown parameters to be calculated, and the function $\mathcal{R}(\xi)$ satisfies the relation

$$\mathcal{R}_\xi^2 = \mathcal{R}^2(1 - \kappa\mathcal{R}^2), \tag{30}$$

and has the following form:

$$\mathcal{R}(\xi) = \frac{4\lambda}{4\lambda^2 \mathrm{e}^{\xi} + \kappa \mathrm{e}^{-\xi}}, \tag{31}$$

where λ represents a constant. Equation (30) fulfills the following equations:

$$\begin{aligned}
&\mathcal{R}_{\xi\xi} = \mathcal{R} - 2\kappa\mathcal{R}^3,\\
&\mathcal{R}_{\xi\xi\xi} = \mathcal{R}_\xi - 6\kappa\mathcal{R}^2\mathcal{R}_\xi,\\
&\mathcal{R}_{\xi\xi\xi\xi} = \mathcal{R} - 20\kappa\mathcal{R}^3 + 24\kappa^2\mathcal{R}^5,\\
&\mathcal{R}_{\xi\xi\xi\xi\xi} = \mathcal{R}_\xi - 60\kappa\mathcal{R}^2\mathcal{R}_\xi + 120\kappa^2\mathcal{R}^4\mathcal{R}_\xi.
\end{aligned} \tag{32}$$

By applying the balancing theory in Eq. (5), the value of the integer n can be determined. Substituting Eqs. (31) and (30) into Eq. (5), and collecting the coefficients of each power of $\mathcal{R}(\xi)$, we obtain a system of algebraic equations with unknown parameters. By setting these coefficients to zero and solving the resulting system, the unknown values can be determined, and finally, the exact solutions of Eq. (5) can be obtained.

3.3. The improved $\mathcal{F}$-expansion scheme

Due to its effectiveness, adaptability, and ability to provide both exact and approximate solutions for nonlinear PDEs, the improved $\mathcal{F}$-expansion method is significant. It serves as a useful tool for researchers in various fields because it supports and simplifies theoretical analysis.

Assume the trial solution of Eq. (5) as

$$v(\xi) = \lambda_0 + \sum_{i=0}^{N} \lambda_i (m + \mathcal{F}(\xi))^i + \sum_{i=1}^{N} \gamma_i (m + \mathcal{F}(\xi))^{-i}, \tag{33}$$

where γ_i and λ_i are not zero at the same time. The following cases are obtained from Eq. (33):

$$\mathcal{F}'(\xi) = q + \mathcal{F}^2(\xi), \tag{34}$$

where q is a constant.

The results of Eq. (34) are as follows:

Case-I If $q < 0$, then

$$\mathcal{F}_1(\xi) = -\sqrt{-q}\tanh(\sqrt{-q}\xi), \tag{35}$$

$$\mathcal{F}_2(\xi) = -\sqrt{-q}\coth(\sqrt{-q}\xi). \tag{36}$$

Case-II If $q > 0$, then

$$\mathcal{F}_3(\xi) = \sqrt{q}\tan(\sqrt{q}\xi), \tag{37}$$

$$\mathcal{F}_4(\xi) = -\sqrt{q}\cot(\sqrt{q}\xi). \tag{38}$$

Case-III If $q = 0$, then

$$\mathcal{F}_5(\xi) = -\frac{1}{\xi}. \tag{39}$$

The balancing theory can be applied to Eq. (5) to determine the value of the integer n. Substituting Eqs. (33) and (34) into Eq. (5), and collecting the coefficients of each power of $\mathcal{F}(\xi)$, we obtain a system of algebraic equations with unknown parameters. By setting these coefficients to zero and solving the resulting system, the unknown parameters can be determined. Finally, the exact solutions of Eq. (5) can be obtained.

3.4. Comparison of the selected methods: applicability and distinctions

Although the three approaches share the same travelling-wave reduction, they differ in their solution ansatz, auxiliary equations, and the resulting functional families:

MSSE method constructs solutions as polynomials in an auxiliary function $\mathcal{S}(\xi)$ satisfying a quartic first-order ODE. This structure naturally yields rich solution families, including hyperbolic, trigonometric, mixed, exponential, and rational-type forms. Its limitation is that it relies on a solvable auxiliary ODE and balancing conditions, and the algebraic complexity may grow rapidly for higher-order models.

New Kudryashov scheme expands the solution in terms of $\mathcal{R}(\xi)$ satisfying $\mathcal{R}_\xi^2 = \mathcal{R}^2(1-\kappa\mathcal{R}^2)$, which typically produces rational–exponential profiles and is well suited for bell-, peakon-, and exponential-type solitary patterns. Its drawback is that the admissible wave families are restricted by the specific structure of $\mathcal{R}(\xi)$, so some oscillatory families may not appear unless the ansatz is further generalized.

Improved $\mathcal{F}$-expansion scheme uses a mixed positive/negative power expansion in $(m+\mathcal{F}(\xi))$ with $\mathcal{F}'(\xi) = q+\mathcal{F}^2(\xi)$, providing a unified approach to periodic (trigonometric), hyperbolic, and rational solutions depending on the sign of q. Its limitation is that parameter constraints can become restrictive, and some solutions may degenerate for special choices of m and q.

Overall, the three methods are connected through the same reduction to an ODE, but they are complementary because each ansatz emphasizes a different auxiliary structure and therefore generates different classes of waveforms.

Remark on the role of Sections 3 and 4 Section 3 summarizes the general algorithms of the three solution techniques for a reduced travelling-wave ODE. In contrast, Section 4 applies these algorithms to the FDENLSM by using the complex wave transformation, reducing the fractional PDE to an explicit ODE, and then deriving method-specific parameter constraints and solution families. Hence, Section 4 is not a repetition of Section 3; rather, it provides the problem-dependent implementation that produces the closed-form wave structures reported in the subsequent sections.

4. Wave transformation of FDENLSM

To obtain general and widely used explicit soliton solutions for the studied model, we employ the three previously mentioned methods in this section. Using the following wave transformation

$$\Lambda = \Theta(\xi)\,\mathrm{e}^{\mathrm{i}\varphi}, \tag{40}$$

where $\xi = \frac{\Gamma(\beta+1)}{\alpha}(x^\alpha + \mu t^\alpha)$, $\varphi = \frac{\Gamma(\beta+1)}{\alpha}(x^\alpha + \delta t^\alpha + \xi_1)$.

The function $\Theta(\xi)$ represents the amplitude component, and the function φ denotes the phase component. Here, μ, δ, and ξ_1 represent the wave number, frequency, and speed of the solitary waves, respectively. When the complex wave assumption is substituted into Eq. (1), it can be separated into real and imaginary parts:

Remark The representation $\Lambda = \Theta(\xi)\,\mathrm{e}^{\mathrm{i}\varphi}$ corresponds to the standard amplitude–phase (polar) form of the complex optical field, where $\Theta(\xi)$ represents the wave amplitude and φ denotes the phase of the optical envelope. In nonlinear optics, the modulus $|\Lambda| = \Theta$ describes the intensity envelope of the propagating pulse, while φ governs the nonlinear phase evolution arising from dispersion and Kerr-type nonlinear effects. After substituting this expression into the governing equation, the resulting relation becomes complex. Separating the real and imaginary parts is therefore a standard mathematical procedure that yields the coupled amplitude and phase evolution equations describing nonlinear wave propagation

$$\begin{cases} Re: \ \Theta(24\delta - 12\wp_1 + 4\wp_3 + \wp_4) - 24\wp_5\Theta^5 + \wp_4\Theta^{(4)} \\ \qquad -24\wp_2\Theta^3 + (12\wp_1 - 12\wp_3 - 6\wp_4)\Theta'' = 0, \\ Im: \ 4(\wp_3+\wp_4)\Theta^{(3)} - 4(6\mu - 6\wp_1 + 3\wp_3 + \wp_4)\Theta' = 0. \end{cases} \tag{41}$$

Consequently, we obtain

$$-\sigma_2\Theta^5 + \sigma_4\Theta^{(4)} + \sigma_3\Theta'' + \sigma_1\Theta + \Theta^3 = 0. \tag{42}$$

where $\mu = -\frac{1}{6}(-6\wp_1 + 3\wp_3 + \wp_4)$, $\wp_3 = -\wp_4$, $\sigma_1 = \frac{-8\delta+4\wp_1+\wp_4}{8\wp_2}$, $\sigma_2 = -\frac{\wp_5}{\wp_2}$, $\sigma_3 = -\frac{2\wp_1+\wp_4}{4\wp_2}$, $\sigma_4 = -\frac{\wp_4}{24\wp_2}$.

4.1. Application of the MSSE method

$N = 1$ can be obtained by applying the balancing principle between the highest power of the nonlinear term Θ^5 in Eq. (42) and the highest-order derivative $\Theta^{(4)}$. Thus, using Eq. (6), we obtain

$$\Theta(\xi) = \gamma_0 + \gamma_1\mathcal{S}(\xi). \tag{43}$$

Substituting Eqs. (43) and (7) into Eq. (42), we obtain an algebraic system of equations by collecting the coefficients of different powers of $\mathcal{S}$. Solving this system, the following solution set is obtained

Family-1

$$\left\{\gamma_0 \to 0,\ \gamma_1 \to \frac{\sqrt{\rho_2}\sqrt[4]{\wp_4}}{\sqrt[4]{\wp_5}},\ \wp_1 \to \frac{\wp_2\sqrt{\wp_4}}{\sqrt{\wp_5}} - \frac{1}{6}(5\rho_1+3)\wp_4,\ \delta \to \frac{1}{24}(9\rho_1^2 - 10\rho_1 - 12\rho_0\rho_2 - 3)\wp_4 - \frac{(\rho_1-1)\wp_2\sqrt{\wp_4}}{2\sqrt{\wp_5}}\right\}. \quad (44)$$

Substituting these values into Eq. (43), we determine abundant solutions for the high-order $(1+1)$ DENLSM.

• If $\rho_0 = 0$, $\rho_1 > 0$, and $\rho_2 \neq 0$, bright and singular solutions are obtained

Cluster 1

$$\Lambda_{1,1}(x,t) = \frac{\sqrt{-\frac{\rho_1}{\rho_2}}\sqrt{\rho_2}\sqrt[4]{\wp_4}\,\mathrm{sech}\left[(\xi+\tau)\sqrt{\frac{\wp_2\sqrt{\wp_4}}{\sqrt{\wp_5}} - \frac{1}{6}(5\rho_1+3)\wp_4}\right]}{\sqrt[4]{\wp_5}} \times \exp\left\{\frac{\mathrm{i}\Gamma(\beta+1)\left\{t^\alpha\left[\frac{9\rho_1^2-10\rho_1-12\rho_0\rho_2-3}{24}\wp_4 - \frac{(\rho_1-1)\wp_2\sqrt{\wp_4}}{2\sqrt{\wp_5}}\right] + x^\alpha\right\}}{\alpha}\right\}. \quad (45)$$

Cluster 2

$$\Lambda_{1,2}(x,t) = \frac{\sqrt{-\frac{\rho_1}{\rho_2}}\sqrt{\rho_2}\sqrt[4]{\wp_4}\,\mathrm{csch}\left(\sqrt{\rho_1}(\xi+\tau)\right)}{\sqrt[4]{\wp_5}} \times \exp\left\{\frac{\mathrm{i}\Gamma(\beta+1)\left\{t^\alpha\left[\frac{9\rho_1^2-10\rho_1-12\rho_0\rho_2-3}{24}\wp_4 - \frac{(\rho_1-1)\wp_2\sqrt{\wp_4}}{2\sqrt{\wp_5}}\right] + x^\alpha\right\}}{\alpha}\right\}. \quad (46)$$

• For constants g_1, g_2, $\rho_0 = 0$, $\rho_1 > 0$, and $\rho_2 = 4g_1g_2$, the combo soliton is obtained as:

Cluster 3

$$\Lambda_{1,3}(x,t) = \frac{4g_1\sqrt{\rho_1}\sqrt{\rho_2}\sqrt[4]{\wp_4}}{\sqrt[4]{\wp_5}(4g_1^2-\rho_2)\left(\sinh(\sqrt{\rho_1}(\xi+\tau)) + \cosh(\sqrt{\rho_1}(\xi+\tau))\right)} \times \exp\left\{\frac{\mathrm{i}\Gamma(\beta+1)\left\{t^\alpha\left[\frac{9\rho_1^2-10\rho_1-12\rho_0\rho_2-3}{24}\wp_4 - \frac{(\rho_1-1)\wp_2\sqrt{\wp_4}}{2\sqrt{\wp_5}}\right] + x^\alpha\right\}}{\alpha}\right\}. \quad (47)$$

• For constants r_1, r_2, $\rho_0 = \frac{\rho_1^2}{4\rho_2}$, $\rho_1 < 0$, and $\rho_2 > 0$, dark and singular soliton solutions are obtained as follows:

Cluster 4

$$\Lambda_{1,4}(x,t) = \frac{\sqrt{-\frac{\rho_1}{\rho_2}}\sqrt{\rho_2}\sqrt[4]{\wp_4}\tanh\left(\frac{\sqrt{-\rho_1}(\xi+\tau)}{\sqrt{2}}\right)}{\sqrt{2}\sqrt[4]{\wp_5}} \times \exp\left\{\frac{\mathrm{i}\Gamma(\beta+1)\left\{t^\alpha\left[\frac{9\rho_1^2-10\rho_1-12\rho_0\rho_2-3}{24}\wp_4 - \frac{(\rho_1-1)\wp_2\sqrt{\wp_4}}{2\sqrt{\wp_5}}\right] + x^\alpha\right\}}{\alpha}\right\}. \quad (48)$$

Cluster 5

$$\Lambda_{1,5}(x,t) = \frac{\sqrt{-\frac{\rho_1}{\rho_2}}\sqrt{\rho_2}\sqrt[4]{\wp_4}\coth\left(\frac{\sqrt{-\rho_1}(\xi+\tau)}{\sqrt{2}}\right)}{\sqrt{2}\sqrt[4]{\wp_5}} \times \exp\left\{\frac{\mathrm{i}\Gamma(\beta+1)\left\{t^\alpha\left[\frac{9\rho_1^2-10\rho_1-12\rho_0\rho_2-3}{24}\wp_4 - \frac{(\rho_1-1)\wp_2\sqrt{\wp_4}}{2\sqrt{\wp_5}}\right] + x^\alpha\right\}}{\alpha}\right\}. \quad (49)$$

The combo-form soliton is given as follows:

Cluster 6

$$\Lambda_{1,6}(x,t) = \frac{\sqrt{-\frac{\rho_1}{\rho_2}}\sqrt{\rho_2}\sqrt[4]{\wp_4}\left(\tanh\left(\frac{\sqrt{-\rho_1}(\xi+\tau)}{\sqrt{2}}\right) + \mathrm{i}\,\mathrm{sech}\left(\sqrt{2}\sqrt{-\rho_1}(\xi+\tau)\right)\right)}{\sqrt{2}\sqrt[4]{\wp_5}}$$

$$\times \exp\left\{\frac{\mathrm{i}\Gamma(\beta+1)\left\{t^{\alpha}\left[\frac{9\rho_1^2-10\rho_1-12\rho_0\rho_2-3}{24}\wp_4-\frac{(\rho_1-1)\wp_2\sqrt{\wp_4}}{2\sqrt{\wp_5}}\right]+x^{\alpha}\right\}}{\alpha}\right\}. \tag{50}$$

Cluster 7

$$\Lambda_{1,7}(x,t) = \frac{\sqrt{-\frac{\rho_1}{\rho_2}}\sqrt{\rho_2}\sqrt[4]{\wp_4}\left(\tanh\left(\frac{\sqrt{-\rho_1}(\xi+\tau)}{2\sqrt{2}}\right)+\coth\left(\frac{\sqrt{-\rho_1}(\xi+\tau)}{2\sqrt{2}}\right)\right)}{2\sqrt{2}\sqrt[4]{\wp_5}}$$
$$\times \exp\left\{\frac{\mathrm{i}\Gamma(\beta+1)\left\{t^{\alpha}\left[\frac{9\rho_1^2-10\rho_1-12\rho_0\rho_2-3}{24}\wp_4-\frac{(\rho_1-1)\wp_2\sqrt{\wp_4}}{2\sqrt{\wp_5}}\right]+x^{\alpha}\right\}}{\alpha}\right\}. \tag{51}$$

Cluster 8

$$\Lambda_{1,8}(x,t) = \frac{\sqrt{-\frac{\rho_1}{\rho_2}}\sqrt{\rho_2}\sqrt[4]{\wp_4}\left(\sqrt{r_1^2+r_2^2}-r_1\cosh\left(\sqrt{2}\sqrt{-\rho_1}(\xi+\tau)\right)\right)}{\sqrt{2}\sqrt[4]{\wp_5}\left(r_1\sinh\left(\sqrt{2}\sqrt{-\rho_1}(\xi+\tau)\right)+r_2\right)}$$
$$\times \exp\left\{\frac{\mathrm{i}\Gamma(\beta+1)\left\{t^{\alpha}\left[\frac{9\rho_1^2-10\rho_1-12\rho_0\rho_2-3}{24}\wp_4-\frac{(\rho_1-1)\wp_2\sqrt{\wp_4}}{2\sqrt{\wp_5}}\right]+x^{\alpha}\right\}}{\alpha}\right\}. \tag{52}$$

Cluster 9

$$\Lambda_{1,9}(x,t) = \frac{\sqrt{-\frac{\rho_1}{\rho_2}}\sqrt{\rho_2}\sqrt[4]{\wp_4}\cosh\left(\sqrt{2}\sqrt{-\rho_1}(\xi+\tau)\right)}{\sqrt{2}\sqrt[4]{\wp_5}\left(\sinh\left(\sqrt{2}\sqrt{-\rho_1}(\xi+\tau)\right)+i\right)}$$
$$\times \exp\left\{\frac{\mathrm{i}\Gamma(\beta+1)\left\{t^{\alpha}\left[\frac{9\rho_1^2-10\rho_1-12\rho_0\rho_2-3}{24}\wp_4-\frac{(\rho_1-1)\wp_2\sqrt{\wp_4}}{2\sqrt{\wp_5}}\right]+x^{\alpha}\right\}}{\alpha}\right\}. \tag{53}$$

• If $\rho_0=0$, $\rho_1<0$, and $\rho_2\neq 0$, trigonometric-form solutions are obtained as follows:

Cluster 10

$$\Lambda_{1,10}(x,t) = \frac{\sqrt{-\frac{\rho_1}{\rho_2}}\sqrt{\rho_2}\sqrt[4]{\wp_4}\sec\left(\sqrt{-\rho_1}(\xi+\tau)\right)}{\sqrt[4]{\wp_5}}$$
$$\times \exp\left\{\frac{\mathrm{i}\Gamma(\beta+1)\left\{t^{\alpha}\left[\frac{9\rho_1^2-10\rho_1-12\rho_0\rho_2-3}{24}\wp_4-\frac{(\rho_1-1)\wp_2\sqrt{\wp_4}}{2\sqrt{\wp_5}}\right]+x^{\alpha}\right\}}{\alpha}\right\}. \tag{54}$$

Cluster 11

$$\Lambda_{1,11}(x,t) = \frac{\sqrt{-\frac{\rho_1}{\rho_2}}\sqrt{\rho_2}\sqrt[4]{\wp_4}\csc\left(\sqrt{-\rho_1}(\xi+\tau)\right)}{\sqrt[4]{\wp_5}}$$
$$\times \exp\left\{\frac{\mathrm{i}\Gamma(\beta+1)\left\{t^{\alpha}\left[\frac{9\rho_1^2-10\rho_1-12\rho_0\rho_2-3}{24}\wp_4-\frac{(\rho_1-1)\wp_2\sqrt{\wp_4}}{2\sqrt{\wp_5}}\right]+x^{\alpha}\right\}}{\alpha}\right\}. \tag{55}$$

• If $\rho_0=\frac{\rho_1^2}{4\rho_2}$, $\rho_1>0$, $\rho_2>0$, and $r_1^2-r_2^2>0$, the trigonometric solutions are obtained as follows:

Cluster 12

$$\Lambda_{1,12}(x,t) = \frac{\sqrt{-\frac{\rho_1}{\rho_2}}\sqrt{\rho_2}\sqrt[4]{\wp_4}\tan\left(\frac{\sqrt{\rho_1}(\xi+\tau)}{\sqrt{2}}\right)}{\sqrt{2}\sqrt[4]{\wp_5}}$$
$$\times \exp\left\{\frac{\mathrm{i}\Gamma(\beta+1)\left\{t^{\alpha}\left[\frac{9\rho_1^2-10\rho_1-12\rho_0\rho_2-3}{24}\wp_4-\frac{(\rho_1-1)\wp_2\sqrt{\wp_4}}{2\sqrt{\wp_5}}\right]+x^{\alpha}\right\}}{\alpha}\right\}. \tag{56}$$

Cluster 13

$$\Lambda_{1,13}(x,t) = \frac{\sqrt{-\frac{\rho_1}{\rho_2}}\sqrt{\rho_2}\sqrt[4]{\wp_4}\cot\left(\frac{\sqrt{\rho_1}(\xi+\tau)}{\sqrt{2}}\right)}{\sqrt{2}\sqrt[4]{\wp_5}} \times\exp\left\{\frac{\mathrm{i}\Gamma(\beta+1)\left\{t^{\alpha}\left[\frac{9\rho_1^2-10\rho_1-12\rho_0\rho_2-3}{24}\wp_4-\frac{(\rho_1-1)\wp_2\sqrt{\wp_4}}{2\sqrt{\wp_5}}\right]+x^{\alpha}\right\}}{\alpha}\right\}. \tag{57}$$

The mixed trigonometric-form solution is given as follows:

Cluster 14

$$\Lambda_{1,14}(x,t) = \frac{\sqrt{-\frac{\rho_1}{\rho_2}}\sqrt{\rho_2}\sqrt[4]{\wp_4}\left(\tan\left(\sqrt{2}\sqrt{\rho_1}(\xi+\tau)\right)-\sec\left(\sqrt{2}\sqrt{\rho_1}(\xi+\tau)\right)\right)}{\sqrt{2}\sqrt[4]{\wp_5}} \times\exp\left\{\frac{\mathrm{i}\Gamma(\beta+1)\left\{t^{\alpha}\left[\frac{9\rho_1^2-10\rho_1-12\rho_0\rho_2-3}{24}\wp_4-\frac{(\rho_1-1)\wp_2\sqrt{\wp_4}}{2\sqrt{\wp_5}}\right]+x^{\alpha}\right\}}{\alpha}\right\}. \tag{58}$$

Cluster 15

$$\Lambda_{1,15}(x,t) = \frac{\sqrt{-\frac{\rho_1}{\rho_2}}\sqrt{\rho_2}\sqrt[4]{\wp_4}\left(\tan\left(\frac{\sqrt{\rho_1}(\xi+\tau)}{2\sqrt{2}}\right)-\cot\left(\frac{\sqrt{\rho_1}(\xi+\tau)}{2\sqrt{2}}\right)\right)}{2\sqrt{2}\sqrt[4]{\wp_5}} \times\exp\left\{\frac{\mathrm{i}\Gamma(\beta+1)\left\{t^{\alpha}\left[\frac{9\rho_1^2-10\rho_1-12\rho_0\rho_2-3}{24}\wp_4-\frac{(\rho_1-1)\wp_2\sqrt{\wp_4}}{2\sqrt{\wp_5}}\right]+x^{\alpha}\right\}}{\alpha}\right\}. \tag{59}$$

Cluster 16

$$\Lambda_{1,16}(x,t) = \frac{\sqrt{-\frac{\rho_1}{\rho_2}}\sqrt{\rho_2}\sqrt[4]{\wp_4}\left(\sqrt{r_1^2-r_2^2}-r_1\cos\left(\sqrt{2}\sqrt{\rho_1}(\xi+\tau)\right)\right)}{\sqrt{2}\sqrt[4]{\wp_5}\left(r_1\sin\left(\sqrt{2}\sqrt{\rho_1}(\xi+\tau)\right)+r_2\right)} \times\exp\left\{\frac{\mathrm{i}\Gamma(\beta+1)\left\{t^{\alpha}\left[\frac{9\rho_1^2-10\rho_1-12\rho_0\rho_2-3}{24}\wp_4-\frac{(\rho_1-1)\wp_2\sqrt{\wp_4}}{2\sqrt{\wp_5}}\right]+x^{\alpha}\right\}}{\alpha}\right\}. \tag{60}$$

Cluster 17

$$\Lambda_{1,17}(x,t) = \frac{\sqrt{-\frac{\rho_1}{\rho_2}}\sqrt{\rho_2}\sqrt[4]{\wp_4}\cos\left(\sqrt{2}\sqrt{\rho_1}(\xi+\tau)\right)}{\sqrt{2}\sqrt[4]{\wp_5}\left(\sin\left(\sqrt{2}\sqrt{\rho_1}(\xi+\tau)\right)-1\right)} \times\exp\left\{\frac{\mathrm{i}\Gamma(\beta+1)\left\{t^{\alpha}\left[\frac{9\rho_1^2-10\rho_1-12\rho_0\rho_2-3}{24}\wp_4-\frac{(\rho_1-1)\wp_2\sqrt{\wp_4}}{2\sqrt{\wp_5}}\right]+x^{\alpha}\right\}}{\alpha}\right\}. \tag{61}$$

• If $\rho_0=0$ and $\rho_1>0$, an exponential solution is obtained as follows:

Cluster 18

$$\Lambda_{1,18}(x,t) = \frac{4\rho_1\sqrt{\rho_2}\sqrt[4]{\wp_4}\exp(\sqrt{\rho_1}(\xi+\tau))}{\sqrt[4]{\wp_5}\left[\exp(2\sqrt{\rho_1}(\xi+\tau))-4\rho_1\rho_2\right]} \times\exp\left\{\frac{\mathrm{i}\Gamma(\beta+1)\left\{t^{\alpha}\left[\frac{9\rho_1^2-10\rho_1-12\rho_0\rho_2-3}{24}\wp_4-\frac{(\rho_1-1)\wp_2\sqrt{\wp_4}}{2\sqrt{\wp_5}}\right]+x^{\alpha}\right\}}{\alpha}\right\}. \tag{62}$$

Cluster 19

$$\Lambda_{1,19}(x,t) = \frac{4\rho_1\sqrt{\rho_2}\sqrt[4]{\wp_4}\exp(\sqrt{\rho_1}(\xi+\tau))}{\sqrt[4]{\wp_5}\left[1-4\rho_1\rho_2\exp(2\sqrt{\rho_1}(\xi+\tau))\right]}$$

$$\times \exp\left\{\frac{\mathrm{i}\Gamma(\beta+1)\left\{t^{\alpha}\left[\frac{9\rho_1^2-10\rho_1-12\rho_0\rho_2-3}{24}\wp_4-\frac{(\rho_1-1)\wp_2\sqrt{\wp_4}}{2\sqrt{\wp_5}}\right]+x^{\alpha}\right\}}{\alpha}\right\}. \tag{63}$$

• If $\rho_0=0$, $\rho_1=0$, and $\rho_2>0$, rational solutions are obtained as follows:

Cluster 20

$$\Lambda_{1,20}(x,t) = \frac{\sqrt[4]{\wp_4}}{\sqrt[4]{\wp_5}(\xi+\tau)}\times \exp\left\{\frac{\mathrm{i}\Gamma(\beta+1)\left\{t^{\alpha}\left[\frac{9\rho_1^2-10\rho_1-12\rho_0\rho_2-3}{24}\wp_4-\frac{(\rho_1-1)\wp_2\sqrt{\wp_4}}{2\sqrt{\wp_5}}\right]+x^{\alpha}\right\}}{\alpha}\right\}. \tag{64}$$

Cluster 21

$$\Lambda_{1,21}(x,t) = \frac{\mathrm{i}\sqrt[4]{\wp_4}}{\sqrt[4]{\wp_5}(\xi+\tau)}\times \exp\left\{\frac{\mathrm{i}\Gamma(\beta+1)\left\{t^{\alpha}\left[\frac{9\rho_1^2-10\rho_1-12\rho_0\rho_2-3}{24}\wp_4-\frac{(\rho_1-1)\wp_2\sqrt{\wp_4}}{2\sqrt{\wp_5}}\right]+x^{\alpha}\right\}}{\alpha}\right\}. \tag{65}$$

where $\xi=\frac{\Gamma(\beta+1)(\mu t^{\alpha}+x^{\alpha})}{\alpha}$.

4.2. Application of the new Kudryashov scheme

According to the new Kudryashov method, Eq. (29) gives

$$\Theta(\xi)=\vartheta_0+\vartheta_1\mathcal{R}(\xi), \tag{66}$$

where ϑ_0 and ϑ_1 are constants. Substituting Eq. (66) and Eq. (31) into Eq. (42), we obtain the following results:

Family-I

$$\left\{\vartheta_0\to 0,\ \vartheta_1\to\frac{\kappa^{2/5}\sqrt[5]{\wp_4}}{\sqrt[5]{\wp_5}},\ \delta\to\frac{1}{8}(4\wp_1+\wp_4)-\frac{(12\wp_1+7\wp_4)\sqrt[5]{\wp_5}}{24\kappa^{2/5}\sqrt[5]{\wp_4}},\ \wp_2\to-\frac{(3\wp_1+4\wp_4)\wp_5^{3/5}}{3\sqrt[5]{\kappa}\wp_4^{3/5}}\right\}.$$

• The peakon soliton solution is obtained as follows:

Cluster 1

$$\begin{aligned}\Lambda_{1,1}(x,t) = {}& \frac{4\kappa^{2/5}\lambda\sqrt[5]{\wp_4}}{\sqrt[5]{\wp_5}\left(\kappa+4\lambda^2\exp\left(\frac{2\Gamma(\beta+1)(\mu t^{\alpha}+x^{\alpha})}{\alpha}\right)\right)}\\ &\times\exp\left\{\frac{\Gamma(\beta+1)\left\{\mathrm{i}\left[\frac{4\wp_1+\wp_4}{8}-\frac{(12\wp_1+7\wp_4)\sqrt[5]{\wp_5}}{24\kappa^{2/5}\sqrt[5]{\wp_4}}\right]t^{\alpha}+\mu t^{\alpha}+(1+\mathrm{i})x^{\alpha}\right\}}{\alpha}\right\}.\end{aligned} \tag{67}$$

Family-II

$$\left\{\begin{aligned}&\vartheta_0\to\frac{\mathrm{i}\sqrt[3]{\frac{5}{3}}\left(\sqrt{34}+5\right)^{5/6}\sqrt{\wp_4}}{4\sqrt[6]{2}\sqrt{\wp_2}\sqrt[6]{-\frac{\kappa\wp_4}{\wp_2}}},\ \vartheta_1\to\frac{\sqrt[3]{\frac{5}{3}\left(\sqrt{34}+5\right)}\sqrt[3]{-\frac{\kappa\wp_4}{\wp_2}}}{2^{2/3}},\ \delta\to\frac{1}{960}\wp_4\left(-\frac{7\times10^{2/3}\sqrt[3]{38343\sqrt{34}+223575}}{\sqrt[3]{-\frac{\kappa\wp_4}{\wp_2}}}-40\left(10\sqrt{34}+63\right)\right),\\ &\wp_1\to-\frac{1}{6}\left(5\sqrt{34}+33\right)\wp_4,\ \wp_5\to\frac{8\sqrt[3]{\frac{2}{3}\left(\sqrt{34}+5\right)}\left(10\sqrt{34}-59\right)\kappa\wp_2}{45\times5^{2/3}\left(-\frac{\kappa\wp_4}{\wp_2}\right)^{2/3}}.\end{aligned}\right.$$

• The exponential solitary wave solution is obtained as follows:

Cluster 2

$$\begin{aligned}\Lambda_{1,2}(x,t) = {}& \left[\frac{2\sqrt[3]{\frac{10}{3}\left(\sqrt{34}+5\right)}\lambda\sqrt[3]{-\frac{\kappa\wp_4}{\wp_2}}\,\mathrm{e}^{\frac{\Gamma(\beta+1)(\mu t^{\alpha}+x^{\alpha})}{\alpha}}}{\kappa+4\lambda^2\,\mathrm{e}^{\frac{2\Gamma(\beta+1)(\mu t^{\alpha}+x^{\alpha})}{\alpha}}}+\frac{\mathrm{i}\left(\sqrt{34}+5\right)^{5/6}\sqrt[3]{\frac{5}{3}}\sqrt{\wp_4}}{4\sqrt[6]{2}\sqrt{\wp_2}\sqrt[6]{-\frac{\kappa\wp_4}{\wp_2}}}\right]\\ &\times\exp\left\{\frac{\mathrm{i}\Gamma(\beta+1)\left\{\frac{\wp_4}{960}\left[-\frac{7\times10^{2/3}\sqrt[3]{38343\sqrt{34}+223575}}{\sqrt[3]{-\frac{\kappa\wp_4}{\wp_2}}}-40(10\sqrt{34}+63)\right]t^{\alpha}+x^{\alpha}\right\}}{\alpha}\right\}.\end{aligned} \tag{68}$$

Family-III

$$\left\{\vartheta_0 \to 0,\ \vartheta_1 \to \frac{\kappa^{2/5}\sqrt[5]{\wp_4}}{\sqrt[5]{\wp_5}},\ \delta \to \frac{3\wp_4^{4/5}\sqrt[5]{\wp_5}}{8\kappa^{2/5}} - \frac{\sqrt[5]{\kappa}\wp_2\wp_4^{3/5}}{2\wp_5^{3/5}} + \frac{\wp_2\wp_4^{2/5}}{2\sqrt[5]{\kappa}\wp_5^{2/5}} - \frac{13\wp_4}{24},\ \wp_1 \to -\frac{\sqrt[5]{\kappa}\wp_2\wp_4^{3/5}}{\wp_5^{3/5}} - \frac{4\wp_4}{3}.\right.$$

• The bell-shaped solitary wave solution is obtained as follows:

Cluster 3

$$\Lambda_{1,3}(x,t) = \frac{4\kappa^{2/5}\lambda\sqrt[5]{\wp_4}}{\sqrt[5]{\wp_5}\left(\kappa + 4\lambda^2 \mathrm{e}^{\frac{2\Gamma(\beta+1)(\mu t^\alpha + x^\alpha)}{\alpha}}\right)} \times \exp\left\{\frac{\Gamma(\beta+1)\left[\mathrm{i}\left(\frac{3\wp_4^{4/5}\sqrt[5]{\wp_5}}{8\kappa^{2/5}} - \frac{\sqrt[5]{\kappa}\wp_2\wp_4^{3/5}}{2\wp_5^{3/5}} + \frac{\wp_2\wp_4^{2/5}}{2\sqrt[5]{\kappa}\wp_5^{2/5}} - \frac{13\wp_4}{24}\right)t^\alpha + \mu t^\alpha + (1+\mathrm{i})x^\alpha\right]}{\alpha}\right\}. \tag{69}$$

4.3. Application of the improved $\mathcal{F}$-expansion scheme

According to the improved $\mathcal{F}$-expansion method, from Eq. (33), we assume that

$$\Theta(\xi) = \lambda_0 + \lambda_1(\mathcal{F}(\xi) + m) + \frac{\gamma_1}{\mathcal{F}(\xi) + m}. \tag{70}$$

Substituting Eq. (70) together with Eq. (34) into Eq. (42), and collecting the coefficients of different powers of $\mathcal{F}(\xi)$, we obtain the following algebraic system. Solving this system gives

Family-I:

$$\begin{cases} \lambda_0 \to \dfrac{m\sqrt[4]{\wp_4}}{\sqrt[4]{\wp_5}},\ \lambda_1 \to 0,\ \gamma_1 \to -\dfrac{\sqrt[4]{\wp_4}(m^2+q)}{\sqrt[4]{\wp_5}}, \\ \delta \to \left(q^2 - \dfrac{5q}{6} - \dfrac{1}{8}\right)\wp_4 + \dfrac{(1-2q)\sqrt{\wp_4}\wp_2}{2\sqrt{\wp_5}}, \\ \wp_1 \to \dfrac{\wp_2\sqrt{\wp_4}}{\sqrt{\wp_5}} - \dfrac{1}{6}(10q+3)\wp_4. \end{cases}$$

Case-I: For $q < 0$, the hyperbolic solutions are obtained as follows:

Cluster 1

$$\Lambda_{1,1}(x,t) = \frac{\sqrt[4]{\wp_4}\left(m - \dfrac{m^2+q}{m - \sqrt{-q}\tanh\left(\frac{\sqrt{-q}\Gamma(\beta+1)(\mu t^\alpha + x^\alpha)}{\alpha}\right)}\right)}{\sqrt[4]{\wp_5}} \times \exp\left\{\frac{\mathrm{i}\Gamma(\beta+1)\left\{t^\alpha\left[\frac{9\rho_1^2 - 10\rho_1 - 12\rho_0\rho_2 - 3}{24}\wp_4 - \frac{(\rho_1-1)\wp_2\sqrt{\wp_4}}{2\sqrt{\wp_5}}\right] + x^\alpha\right\}}{\alpha}\right\}. \tag{71}$$

Cluster 2

$$\Lambda_{1,2}(x,t) = \frac{\sqrt[4]{\wp_4}\left(m - \dfrac{m^2+q}{m - \sqrt{-q}\coth\left(\frac{\sqrt{-q}\Gamma(\beta+1)(\mu t^\alpha + x^\alpha)}{\alpha}\right)}\right)}{\sqrt[4]{\wp_5}} \times \exp\left\{\frac{\mathrm{i}\Gamma(\beta+1)\left\{t^\alpha\left[\frac{9\rho_1^2 - 10\rho_1 - 12\rho_0\rho_2 - 3}{24}\wp_4 - \frac{(\rho_1-1)\wp_2\sqrt{\wp_4}}{2\sqrt{\wp_5}}\right] + x^\alpha\right\}}{\alpha}\right\}. \tag{72}$$

Case-II: For $q > 0$, the trigonometric solutions are obtained as follows:

Cluster 3

$$\Lambda_{1,3}(x,t) = \frac{\sqrt[4]{\wp_4}\left(m\sqrt{q}\tan\left(\frac{\sqrt{q}\Gamma(\beta+1)(\mu t^\alpha + x^\alpha)}{\alpha}\right) - q\right)}{\sqrt[4]{\wp_5}\left(m + \sqrt{q}\tan\left(\frac{\sqrt{q}\Gamma(\beta+1)(\mu t^\alpha + x^\alpha)}{\alpha}\right)\right)}$$

$$\times \exp\left\{\frac{\mathrm{i}\Gamma(\beta+1)\left\{t^{\alpha}\left[\frac{9\rho_1^2-10\rho_1-12\rho_0\rho_2-3}{24}\wp_4-\frac{(\rho_1-1)\wp_2\sqrt{\wp_4}}{2\sqrt{\wp_5}}\right]+x^{\alpha}\right\}}{\alpha}\right\}. \tag{73}$$

Cluster 4

$$\Lambda_{1,4}(x,t) = -\frac{\sqrt[4]{\wp_4}\left(m\sqrt{q}\cot\left(\frac{\sqrt{q}\Gamma(\beta+1)(\mu t^{\alpha}+x^{\alpha})}{\alpha}\right)+q\right)}{\sqrt[4]{\wp_5}\left(m-\sqrt{q}\cot\left(\frac{\sqrt{q}\Gamma(\beta+1)(\mu t^{\alpha}+x^{\alpha})}{\alpha}\right)\right)} \times \exp\left\{\frac{\mathrm{i}\Gamma(\beta+1)\left\{t^{\alpha}\left[\frac{9\rho_1^2-10\rho_1-12\rho_0\rho_2-3}{24}\wp_4-\frac{(\rho_1-1)\wp_2\sqrt{\wp_4}}{2\sqrt{\wp_5}}\right]+x^{\alpha}\right\}}{\alpha}\right\}. \tag{74}$$

Case-III: For $q=0$, the rational solution is obtained as follows:

Cluster 5

$$\Lambda_{1,5}(x,t) = -\frac{\sqrt[4]{\wp_4}\left[\alpha m+q\Gamma(\beta+1)(\mu t^{\alpha}+x^{\alpha})\right]}{\sqrt[4]{\wp_5}\left[m\Gamma(\beta+1)(\mu t^{\alpha}+x^{\alpha})-\alpha\right]} \times \exp\left\{\frac{\mathrm{i}\Gamma(\beta+1)\left\{t^{\alpha}\left[\frac{9\rho_1^2-10\rho_1-12\rho_0\rho_2-3}{24}\wp_4-\frac{(\rho_1-1)\wp_2\sqrt{\wp_4}}{2\sqrt{\wp_5}}\right]+x^{\alpha}\right\}}{\alpha}\right\}. \tag{75}$$

Family-II

$$\begin{cases} \lambda_1 \to 0, \qquad \gamma_1 \to -\dfrac{\lambda_0(m^2+q)}{m}, \\ \delta \to \dfrac{\lambda_0^2(1-2q)\wp_2}{2m^2}+\dfrac{4q(6q-5)-3}{24}\wp_4, \\ \wp_1 \to \dfrac{\lambda_0^2\wp_2}{m^2}-\dfrac{10q+3}{6}\wp_4, \qquad \wp_5 \to \dfrac{m^4\wp_4}{\lambda_0^4}. \end{cases} \tag{76}$$

Case-I: For $q<0$, the hyperbolic solutions are obtained as follows:

Cluster 6

$$\Lambda_{1,6}(x,t) = \lambda_0\left(1-\frac{m^2+q}{m^2-m\sqrt{-q}\tanh\left(\frac{\sqrt{-q}\Gamma(\beta+1)(\mu t^{\alpha}+x^{\alpha})}{\alpha}\right)}\right) \times \exp\left\{\frac{\mathrm{i}\Gamma(\beta+1)\left\{t^{\alpha}\left[\frac{\lambda_0^2(1-2q)\wp_2}{2m^2}+\frac{4q(6q-5)-3}{24}\wp_4\right]+x^{\alpha}\right\}}{\alpha}\right\}. \tag{77}$$

Cluster 7

$$\Lambda_{1,7}(x,t) = \lambda_0\left(1-\frac{m^2+q}{m^2-m\sqrt{-q}\coth\left(\frac{\sqrt{-q}\Gamma(\beta+1)(\mu t^{\alpha}+x^{\alpha})}{\alpha}\right)}\right) \times \exp\left\{\frac{\mathrm{i}\Gamma(\beta+1)\left\{t^{\alpha}\left[\frac{\lambda_0^2(1-2q)\wp_2}{2m^2}+\frac{4q(6q-5)-3}{24}\wp_4\right]+x^{\alpha}\right\}}{\alpha}\right\}. \tag{78}$$

Case-II: For $q>0$, the trigonometric solutions are obtained as follows:

Cluster 8

$$\Lambda_{1,8}(x,t) = \lambda_0\left(1-\frac{m^2+q}{m^2+m\sqrt{q}\tan\left(\frac{\sqrt{q}\Gamma(\beta+1)(\mu t^{\alpha}+x^{\alpha})}{\alpha}\right)}\right) \times \exp\left\{\frac{\mathrm{i}\Gamma(\beta+1)\left\{t^{\alpha}\left[\frac{\lambda_0^2(1-2q)\wp_2}{2m^2}+\frac{4q(6q-5)-3}{24}\wp_4\right]+x^{\alpha}\right\}}{\alpha}\right\}. \tag{79}$$

Cluster 9

$$\Lambda_{1,9}(x,t) = \lambda_0\left(1-\frac{m^2+q}{m^2-m\sqrt{q}\cot\left(\frac{\sqrt{q}\Gamma(\beta+1)(\mu t^\alpha+x^\alpha)}{\alpha}\right)}\right) \times\exp\left\{\frac{\mathrm{i}\Gamma(\beta+1)\left\{t^\alpha\left[\frac{\lambda_0^2(1-2q)\wp_2}{2m^2}+\frac{4q(6q-5)-3}{24}\wp_4\right]+x^\alpha\right\}}{\alpha}\right\}. \tag{80}$$

Case-III: For $q=0$, the rational solution is obtained as follows:

Cluster 10

$$\Lambda_{1,10}(x,t) = -\frac{\lambda_0(\alpha m+q\Gamma(\beta+1)(\mu t^\alpha+x^\alpha))}{m(m\Gamma(\beta+1)(\mu t^\alpha+x^\alpha)-\alpha)} \times\exp\left\{\frac{\mathrm{i}\Gamma(\beta+1)\left\{t^\alpha\left[\frac{\lambda_0^2(1-2q)\wp_2}{2m^2}+\frac{4q(6q-5)-3}{24}\wp_4\right]+x^\alpha\right\}}{\alpha}\right\}. \tag{81}$$

5. MI

In this part, we study the MI of the proposed model using the linear stability analysis. MI is a phenomenon in nonlinear systems where small perturbations to a continuous wave solution grow exponentially over time. The linear stability method involves linearizing the governing equation around a continuous wave solution and analyzing the growth rates of small perturbations using linear stability theory. This analysis typically involves solving a linear eigenvalue problem to determine the spectrum of growth rates associated with different perturbation modes. Assume that the proposed M-fractional model has the following stable solution:[32]

$$\Lambda(x,t) = a_0\,\mathrm{e}^{\mathrm{i}\varphi t^\alpha}. \tag{82}$$

The real constant a_0 in this instance is arbitrary. $\varphi=\frac{(a_0^4\wp_5+a_0^2\wp_2)\Gamma(\beta+1)}{\alpha}$ is obtained by substituting Eq. (82) into Eq. (1). Taking into account the subsequent perturbed stationary solution

$$\Lambda(x,t) = (a_0+\varepsilon\mathcal{V}(x,t))\exp\left[\frac{\left(a_0^4\wp_5+a_0^2\wp_2\right)\Gamma(\beta+1)t^\alpha}{\alpha}\right], \tag{83}$$

where $\mathcal{V}$ signifies a fractional complex function. From Eqs. (83) and (1), the outcomes fulfil the following linear equation:

$$24\mathrm{i}D_{M,t}^{\alpha,\beta}\mathcal{V}+(96a_0^4\wp_5+48a_0^2\wp_2)(\mathcal{V}+\mathcal{V}^*) -4\wp_1D_{M,x}^{2\alpha,\beta}\mathcal{V}-4\mathrm{i}\wp_3D_{M,x}^{3\alpha,\beta}\mathcal{V}-\wp_4D_{M,x}^{4\alpha,\beta}\mathcal{V}=0, \tag{84}$$

where $*$ refers to the conjugate function, and hence Eq. (84) has the following form:

$$\mathcal{V}(x,t) = v_1\,\mathrm{e}^{\mathrm{i}(\eta x^\alpha-\varpi t^\alpha)}+v_2\,\mathrm{e}^{-\mathrm{i}(\eta x^\alpha-\varpi t^\alpha)}, \tag{85}$$

where η denotes the complex frequency, ϖ is the real disturbance wave number, and v_1, v_2 denote the coefficients of the linear combination. Combining and substituting Eq. (85) into Eq. (84) yields the following system of equations:

$$\begin{pmatrix}a_{11} & a_{12}\\ a_{21} & a_{22}\end{pmatrix}\begin{pmatrix}v_1\\ v_2\end{pmatrix}=\begin{pmatrix}0\\0\end{pmatrix}, \tag{86}$$

$$\begin{aligned}
&48a_0^2\wp_2+96a_0^4\wp_5-\frac{\alpha^4\eta^4\wp_4}{\Gamma(\beta+1)^4}-\frac{4\alpha^3\eta^3\wp_3}{\Gamma(\beta+1)^3}\\
&\quad+\frac{4\alpha^2\eta^2\wp_1}{\Gamma(\beta+1)^2}+\frac{24\alpha\varpi}{\Gamma(\beta+1)}=0,\\
&96a_0^4\wp_5+48a_0^2\wp_2=0,\\
&96a_0^4\wp_5+8a_0^2\wp_2=0,\\
&48a_0^2\wp_2+96a_0^4\wp_5-\frac{\alpha^4\eta^4\wp_4}{\Gamma(\beta+1)^4}+\frac{4\alpha^3\eta^3\wp_3}{\Gamma(\beta+1)^3}\\
&\quad+\frac{4\alpha^2\eta^2\wp_1}{\Gamma(\beta+1)^2}-\frac{24\alpha\varpi}{\Gamma(\beta+1)}=0.
\end{aligned} \tag{87}$$

When evaluating the determinant and setting the outcome to zero, the relationship is obtained as follows:

$$\begin{aligned}
&\alpha^8\eta^8\wp_4^2-8\alpha^6\eta^6\left(2\wp_3^2+\wp_1\wp_4\right)\Gamma(\beta+1)^2+16\alpha^4\eta^3\Gamma\\
&\quad\times(\beta+1)^4\left[-6a_0^2\eta\wp_4\left(2a_0^2\wp_5+\wp_2\right)+\eta\wp_1^2+12\varpi\wp_3\right]\\
&\quad+192\alpha^2\Gamma(\beta+1)^6\left[2a_0^2\eta^2\wp_1\left(2a_0^2\wp_5+\wp_2\right)-3\varpi^2\right]\\
&\quad=0,
\end{aligned} \tag{88}$$

The key to understanding modulation instability lies in the dispersion relation of the system, which describes how the wave vector of perturbations depends on their frequency. In many cases, the dispersion relation exhibits regions of anomalous dispersion, where the group velocity is opposite to the phase velocity. These regions are often associated with the onset of modulation instability. By considering Eq. (88), we can analyze the dispersion relation of Eq. (1) as follows:

$$\varpi = \frac{4\alpha^2\eta^3\wp_3\Gamma(\beta+1)^4 + \sqrt{\eta^2\Gamma(\beta+1)^6\left[\alpha^2\eta^2\wp_4 - 4\wp_1\Gamma(\beta+1)^2\right]\left[\alpha^4\eta^4\wp_4 - 4\alpha^2\eta^2\wp_1\Gamma(\beta+1)^2 - 96a_0^2\left(2a_0^2\wp_5+\wp_2\right)\Gamma(\beta+1)^4\right]}}{24\Gamma(\beta+1)^6}. \tag{89}$$

Equation (89) yields the steady-state stability for Eq. (1) when

$$\eta^2\Gamma(\beta+1)^6\alpha^2\eta^2\wp_4 - 4\wp_1\Gamma(\beta+1)^2\left[\alpha^4\eta^4\wp_4 - 4\alpha^2\eta^2\wp_1\Gamma(\beta+1)^2 - 96a_0^2\left(2a_0^2\wp_5+\wp_2\right)\Gamma(\beta+1)^4\right] \geq 0. \tag{90}$$

The MI in Eq. (1) occurs when η is an imaginary wave number.

$$\eta^2\Gamma(\beta+1)^6\alpha^2\eta^2\wp_4 - 4\wp_1\Gamma(\beta+1)^2\left[\alpha^4\eta^4\wp_4 - 4\alpha^2\eta^2\wp_1\Gamma(\beta+1)^2 - 96a_0^2\left(2a_0^2\wp_5+\wp_2\right)\Gamma(\beta+1)^4\right] < 0. \tag{91}$$

MI is a fundamental nonlinear phenomenon that arises in various physical systems, and its analysis using the linear stability method is essential for understanding its onset and dynamics. In Figs. 1 and 2, the modulation instability (MI) growth rate, or gain, is found by the maximum absolute value of the imaginary part of the wave number. This can be done as follows:

$$G(M) = 2\mathrm{Im}(w) = 2\mathrm{Im}\left[-\frac{m\sqrt{\wp_1-4\wp_3}\sqrt{\alpha^2m^2\left(\wp_1-4\wp_3\right)-4a_0^2\wp_2\Gamma(\beta+1)^2}}{\Gamma(\beta+1)}\right]. \tag{92}$$

In this case, the MI gain is significantly impacted by the incident power a_0.

It is worth noting that the fractional-order parameters α and β play important roles in determining the stability characteristics of the system. These parameters appear explicitly in the dispersion relation and the modulation instability gain spectrum through the factors involving $\Gamma(\beta+1)$ and the fractional temporal scaling t^α. Variations in α modify the effective temporal evolution of the perturbation modes, thereby influencing the growth rate of instability. Similarly, the parameter β affects the strength of the fractional operator through the Mittag–Leffler function, which alters the dispersion balance of the system. Consequently, different choices of (α,β) lead to noticeable changes in the MI gain profiles, as illustrated in Figs. 1 and 2.

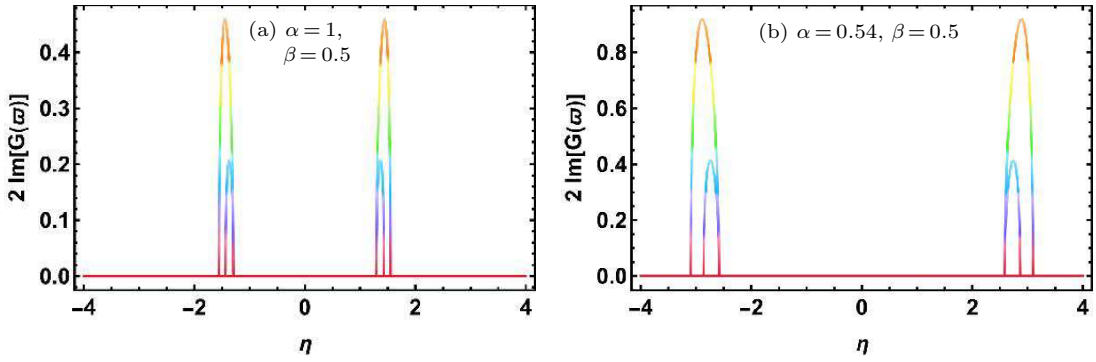


Fig. 1. MI regions for different values of $a_0 = \{0.14, 0.25, 0.36\}$, with $\wp_1 = 2.34$, $\wp_2 = 0.87$, $\wp_3 = 0.13$, $\wp_4 = 4.4$, and $\wp_5 = 0.5$ from left to right, respectively.

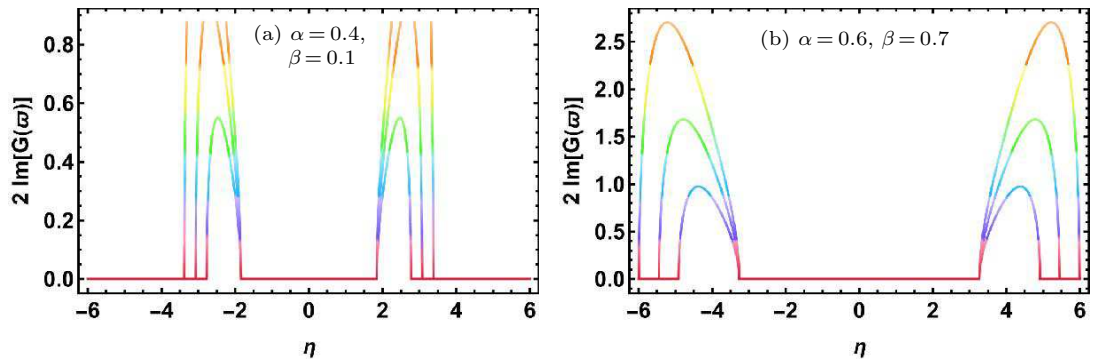


Fig. 2. MI regions for different values of $a_0 = \{0.4, 0.5, 0.6\}$, with $\wp_1 = 0.34$, $\wp_2 = 0.7$, $\wp_3 = 0.3$, $\wp_4 = 0.4$, and $\wp_5 = 0.5$ from left to right, respectively.

6. Results and discussion

In this part, the unique contribution of this research is synthesized by applying multifaceted analytical techniques, namely, the MSSE method, the new Kudryashov approach, and the improved $\mathcal{F}$-expansion method, to the high-order FDENLSM. Thus, by establishing the mentioned techniques, we find novel soliton solutions such as bright, singular, combo, dark, mixed trigonometric, periodic, W-shaped, bell-shaped, peakon-shaped, exponential, rational, and hyperbolic solitary waves. These thorough analyses of soliton solutions provide fresh insights into the applications of nonlinear dispersive waves when high-order chromatic effects are present. In addition, these methods are used to create new soliton wave patterns, which helps us explore the unique dynamical characteristics and topological properties of solitary waves. For evaluating the model's physical properties, elucidating nonlinear behavior, and confirming the precision of analytical methods, solitary wave solution graphs are essential tools. Also, the MI of the governed model is investigated. The literature has evaluated and compared these results with earlier findings obtained from other approaches. A unique structure was shown by Eq. (1); it searches for more interesting, broadly applicable, and unique soliton waveforms. Physical interpretation is the process of comprehending and elucidating mathematical models or solutions in terms of actual physical processes or events.

The three methodologies employed in this work provide complementary perspectives for analyzing the considered nonlinear model. The MSSE approach offers an efficient analytical framework for constructing exact travelling-wave solutions and identifying multiple families of nonlinear structures. However, its applicability generally depends on the existence of suitable auxiliary equations and balance conditions. The neural-symbolic computational framework is useful for verifying solution structures and exploring complex parameter regimes, although it may require careful parameter tuning and computational resources. Finally, the dynamical and graphical analyses provide important qualitative insight into wave propagation and stability features, but they primarily offer numerical or visual interpretation rather than closed-form analytical expressions. Together, these approaches provide a more comprehensive understanding of the nonlinear dynamics of the proposed system.

The analytical solutions obtained in this study are visualized in Figs. 3–16, which provide graphical representations of the derived wave structures and illustrate the diverse nonlinear behaviors generated by the governing model. Figure presents the bright-type soliton solution of Eq. (45) obtained through the MSSE approach, representing a localized wave packet with a concentrated amplitude peak. The combo structure of Eq. (47) is depicted in Fig. 4, showing the interaction of different nonlinear modes within a single wave profile. In Fig. 5, the dark-type solution of Eq. (48) is illustrated,

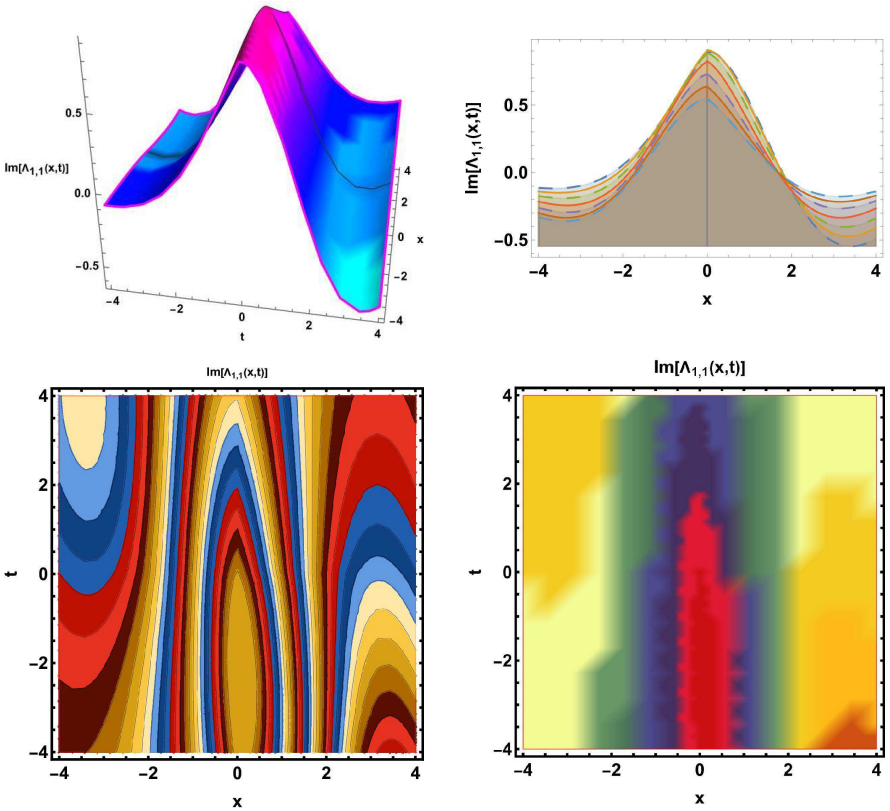


Fig. 3. Physical visualization of the bright-type solution of Eq. (45) for $\rho_0 = 0$, $\rho_1 = 0.6$, $\rho_2 = 0.7$, $\wp_2 = 0.8$, $\wp_4 = 0.9$, $\wp_5 = 0.5$, $\alpha = 0.9$, $\beta = 0.4$, $\tau = 1$, and $\mu = 0.6$.

describing a localized intensity dip propagating over a nonzero background. Figure 6 demonstrates the hyperbolic-type solution of Eq. (50), which characterizes solitary wave propagation governed by nonlinear and dispersive effects. The periodic soliton structure of Eq. (52) is shown in Fig. 7, indicating regular oscillatory wave patterns in the spatial domain. Figure 8 displays the periodic W-form (or combo-type) solution of Eq. (58), revealing a multi-peaked wave structure generated by the interaction of periodic nonlinear components.

The exponential-type solution of Eq. (62) is presented in Fig. 9, reflecting rapidly varying wave profiles controlled by exponential growth or decay mechanisms. Figure illustrates the peakon-type structure of Eq. (67), which exhibits a sharply localized crest typical of peaked solitary waves. The periodic solution of Eq. (68) is depicted in Fig. 11, representing regular oscillatory wave dynamics arising from the interplay of dispersion and nonlinearity. Figure 12 demonstrates the bell-shaped solution of Eq. (69), corresponding to a smooth localized solitary wave profile. The singular solution of Eq. (72) is illustrated in Fig. 13, showing the emergence of sharp amplitude variations characteristic of singular wave structures. In Fig. 14, the periodic wave pattern of Eq. (73) is displayed, revealing repeating oscillatory structures in the wave field. Figure presents the dark-type structure of Eq. (77), highlighting localized depressions within the wave profile. Finally, Figure depicts the rational solution of Eq. (81), which exhibits algebraically localized wave patterns often associated with rational wave dynamics.

These graphical illustrations confirm that the proposed high-order FDENLSM can capture a wide spectrum of nonlinear dispersive wave phenomena observed in modern nonlinear physical systems.

To further interpret the obtained results from the perspective of nonlinear optics, the derived waveforms can be classified into several physically distinct solution families that correspond to different propagation behaviors of optical pulses in nonlinear dispersive media.

Bright, bell-shaped, and peakon solutions correspond to localized high-intensity optical pulses formed when the nonlinear self-focusing effect compensates for group-velocity dispersion. Such structures are typical in anomalous-dispersion regimes of optical fibers and represent stable soliton envelopes used in pulse transmission and optical signal propagation.

Dark structures represent localized intensity depressions on a continuous-wave background and are commonly associated with self-defocusing nonlinear media and normal-dispersion regimes. These waves often describe phase defects or intensity dips propagating through optical fields.

Periodic and trigonometric waveforms correspond to repeating oscillatory wave trains that arise from the interplay between dispersion and nonlinear phase modulation. In nonlinear optics, such structures may represent modulated optical fields or intermediate states between continuous waves and isolated solitons.

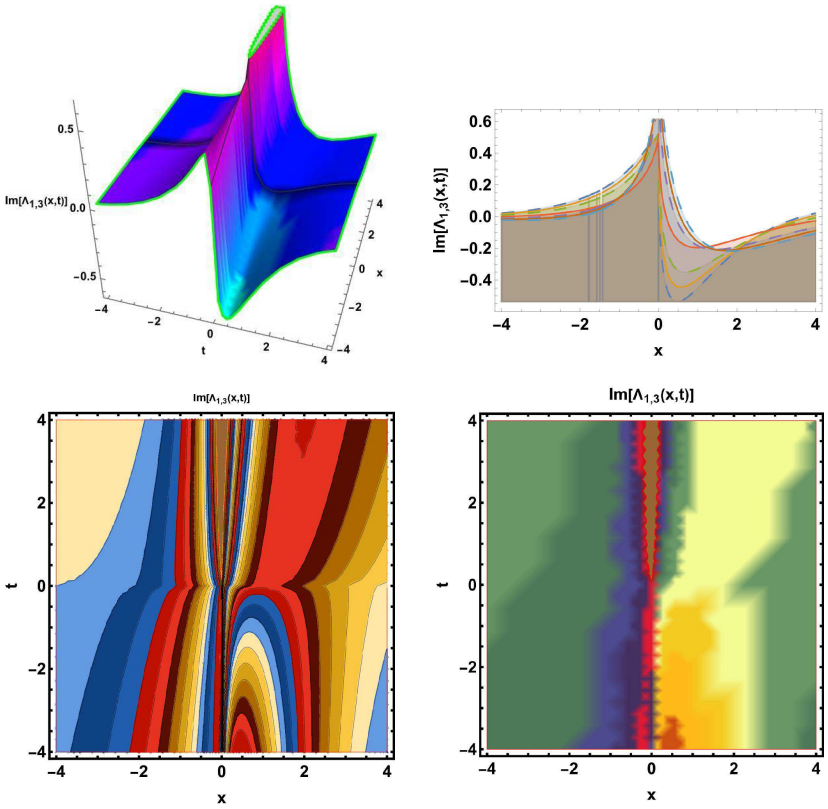


Fig. 4. Physical visualization of the combo-type solution of Eq. (47) for $\rho_0 = 0$, $\rho_1 = 0.44$, $g_1 = 1$, $g_2 = 2.4$, $\wp_2 = 0.8$, $\wp_4 = 0.9$, $\wp_5 = -0.88$, $\alpha = 0.5$, $\beta = 0.4$, $\tau = 1$, and $\mu = 0.08$.

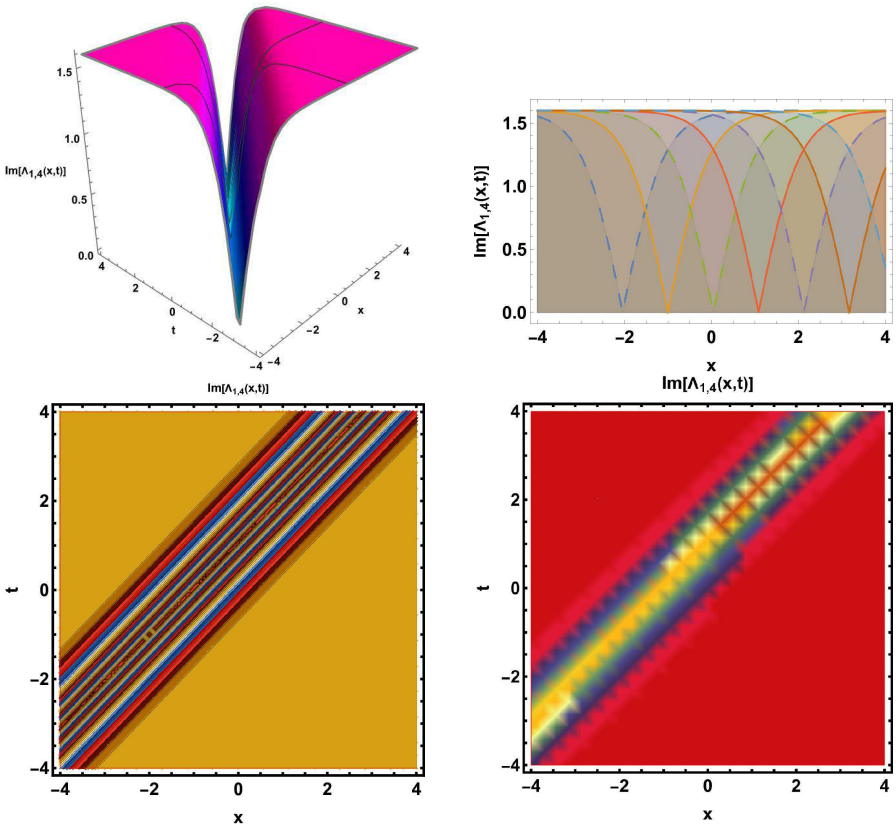


Fig. 5. Physical visualization of the dark-type solution of Eq. (48) for $\rho_1 = -2.7$, $\rho_2 = 1.4$, $\wp_2 = 1.9$, $\wp_4 = 1.8$, $\wp_5 = 0.5$, $\tau = 1$, $\mu = -0.96$, $\alpha = 1$, and $\beta = 0.9$.

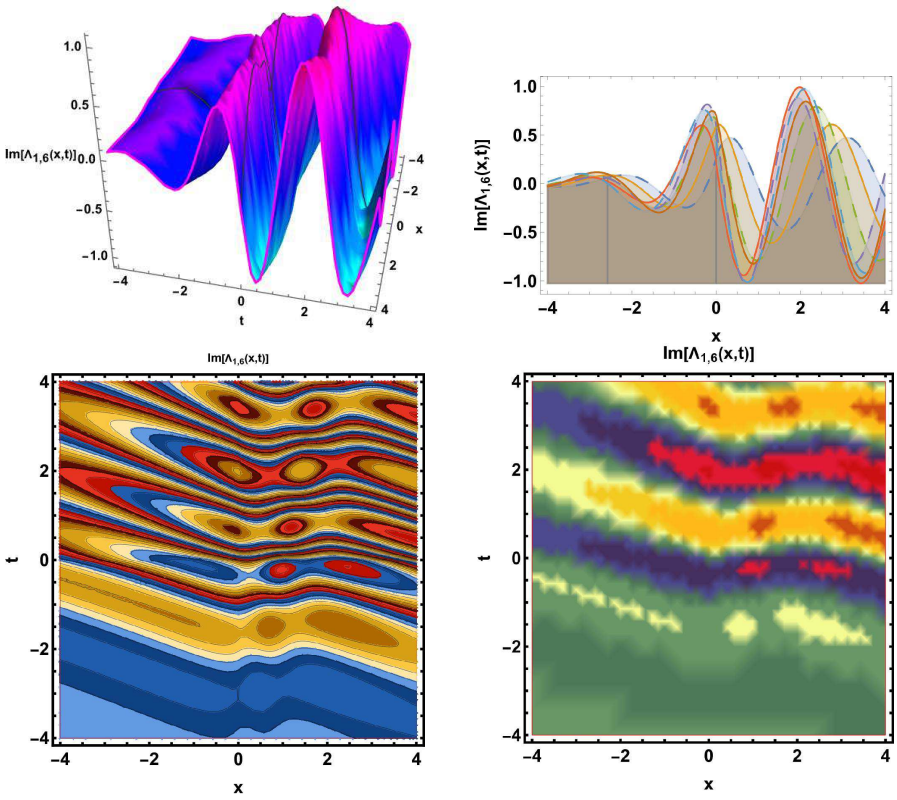


Fig. 6. Physical visualization of the hyperbolic-type solution of Eq. (50) for $\rho_1 = -2.7$, $\rho_2 = 0.4$, $\wp_2 = 0.9$, $\wp_4 = 0.3$, $\wp_5 = 0.41$, $\mu = -0.2$, $\alpha = 0.9$, $\beta = 0.4$, and $\tau = -1$.

Hyperbolic solutions represent strongly localized solitary waves formed through the balance between nonlinear and dispersive effects, describing stable optical pulse propagation in nonlinear transmission media. Singular solutions capture extreme-gradient events and steep wavefronts, which may correspond to strong focusing regimes or instability limits in nonlinear optical

systems where the field intensity changes abruptly. Exponential profiles characterize rapidly varying wave envelopes, often associated with dispersion-dominated pulse reshaping or strong amplitude modulation during propagation.

Rational solutions exhibit algebraically localized structures that are often linked to rogue-wave-type optical events or strongly localized bursts generated by modulation instability.

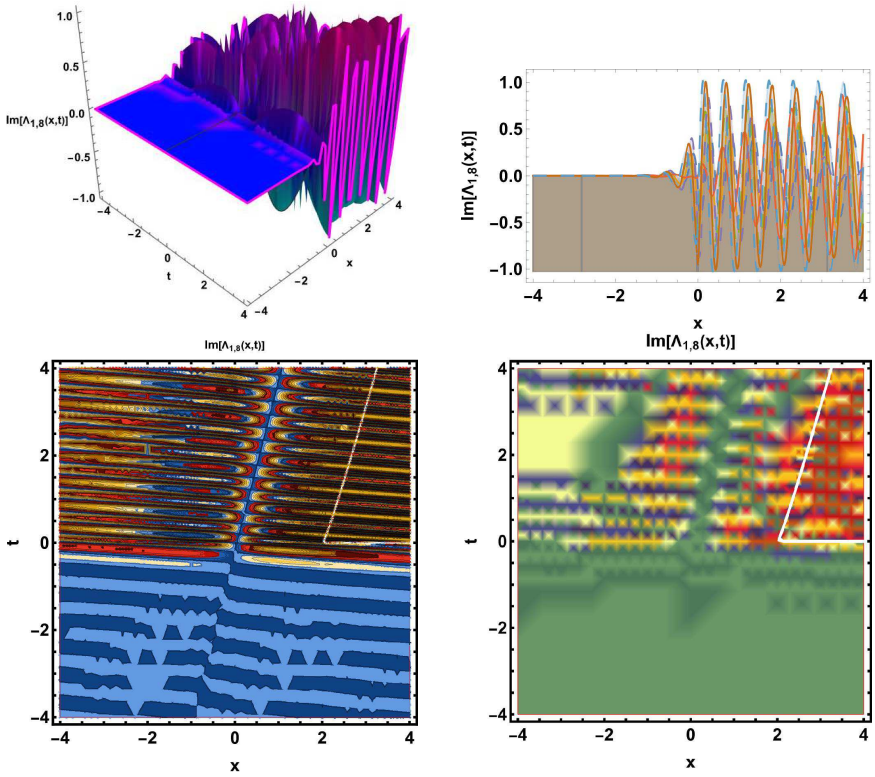


Fig. 7. Physical visualization of the periodic W-form solution of Eq. (58) for $\rho_1 = 0.9$, $\rho_2 = 0.82$, $\wp_2 = 0.5$, $\wp_4 = 0.3$, $\wp_5 = 2.21$, $\alpha = 0.85$, $\beta = 0.2$, $\mu = -0.8$, and $\tau = 0.1$.

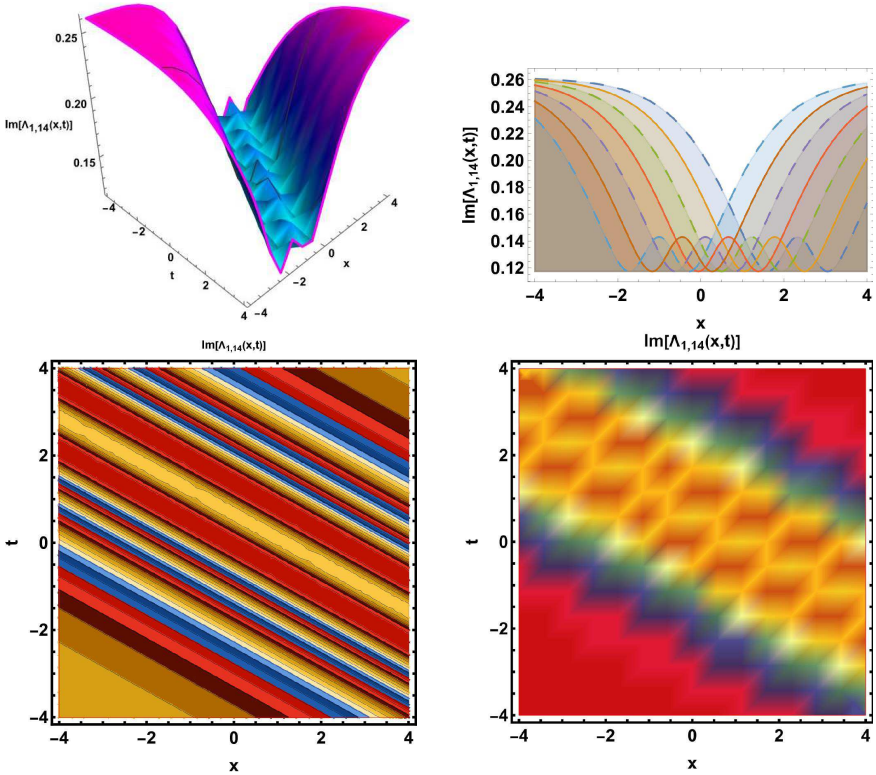


Fig. 8. Physical visualization of the periodic W-form solution of Eq. (58) for $\rho_1 = 0.9$, $\rho_2 = 0.82$, $\wp_2 = 0.5$, $\wp_4 = 0.3$, $\wp_5 = 2.21$, $\alpha = 0.85$, $\beta = 0.2$, $\mu = -0.8$, and $\tau = 0.1$.

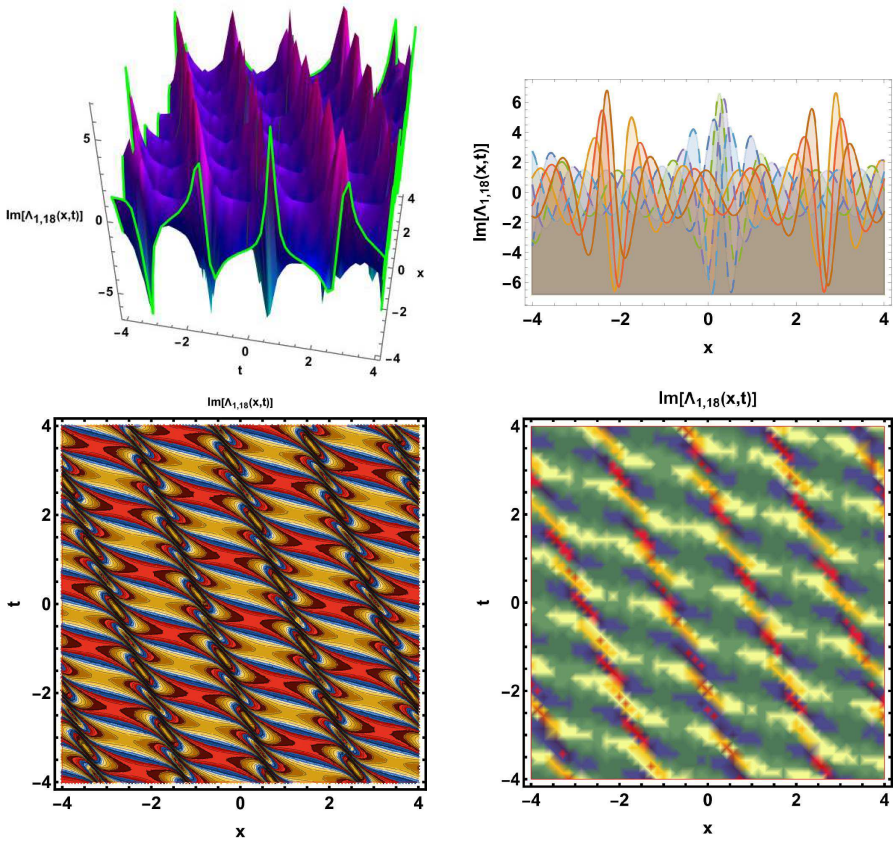


Fig. 9. Physical visualization of the exponential-type solution of Eq. (62) for $\rho_0 = 0$, $\rho_1 = -2.99$, $\rho_2 = 0.13$, $\wp_2 = 0.5$, $\wp_4 = 1$, $\wp_5 = 1.71$, $\alpha = 1$, $\beta = 0.8$, $\mu = 0.4$, and $\tau = -0.1$.

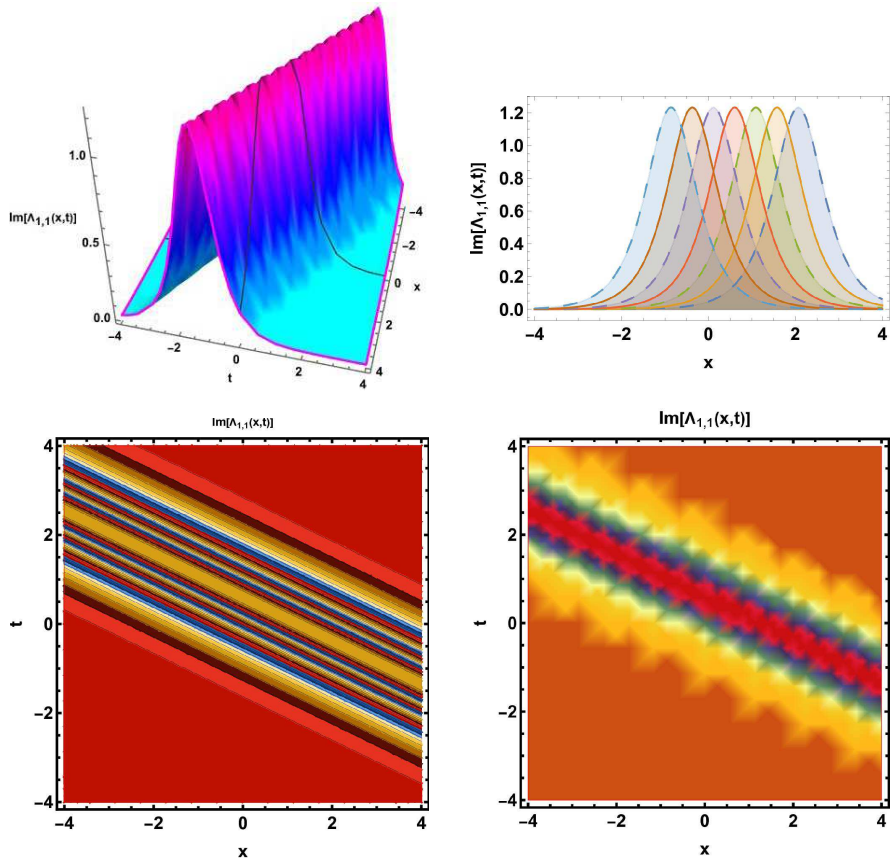


Fig. 10. Physical visualization of the peakon-type solution of Eq. (67) for $\kappa = 4\lambda$, $\lambda = 0.1$, $\wp_1 = 0.4$, $\wp_2 = 0.8$, $\wp_4 = 0.9$, $\wp_5 = 0.5$, $\alpha = 1$, $\beta = 0.8$, and $\mu = 2.05$.

Finally, combo and W-form solutions illustrate the interaction or coexistence of multiple nonlinear modes within a single wave envelope, which in nonlinear optics may correspond to bound-state solitons or multi-peak pulse structures influenced by higher-order dispersion and nonlinear effects.

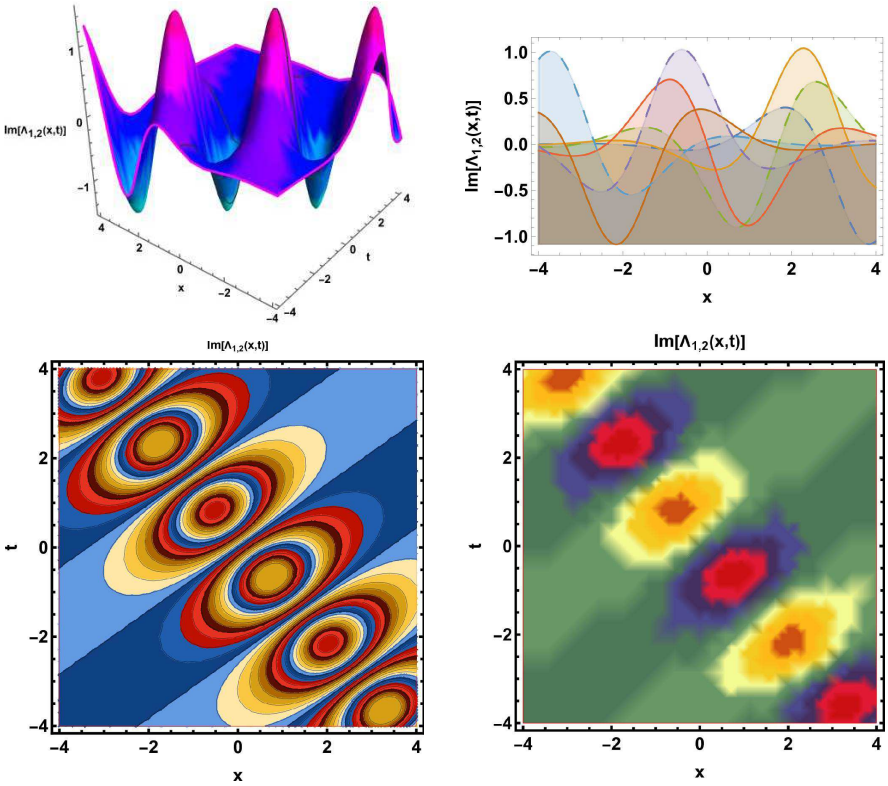


Fig. 11. Physical visualization of the periodic-type solution of Eq. (68) for $\kappa = 4\lambda$, $\lambda = 0.7$, $\wp_1 = 0.5$, $\wp_2 = -0.4$, $\wp_4 = 0.19$, $\wp_5 = 0.9$, $\alpha = 1$, $\beta = 0.8$, and $\mu = 0.85$.

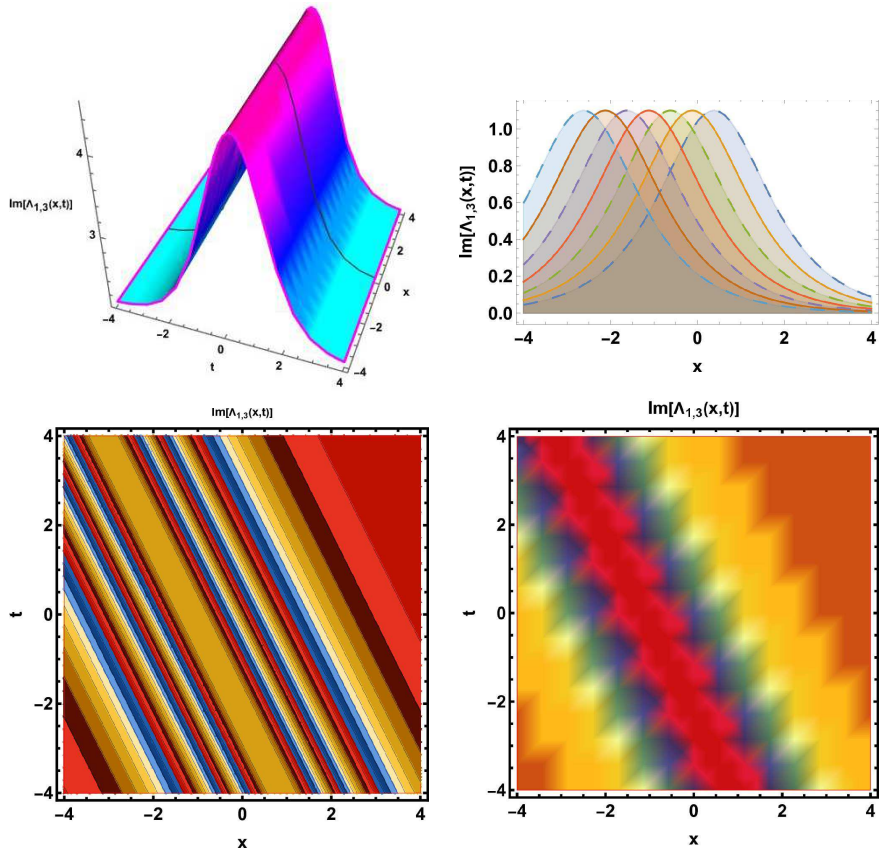


Fig. 12. Physical visualization of the bell-type solution of Eq. (69) for $\kappa = 4$, $\lambda = -2.7$, $\wp_1 = 0.5$, $\wp_2 = 0.4$, $\wp_4 = 2.9$, $\wp_5 = 0.9$, $\alpha = 1$, $\beta = 0.5$, and $\mu = 0.5$.

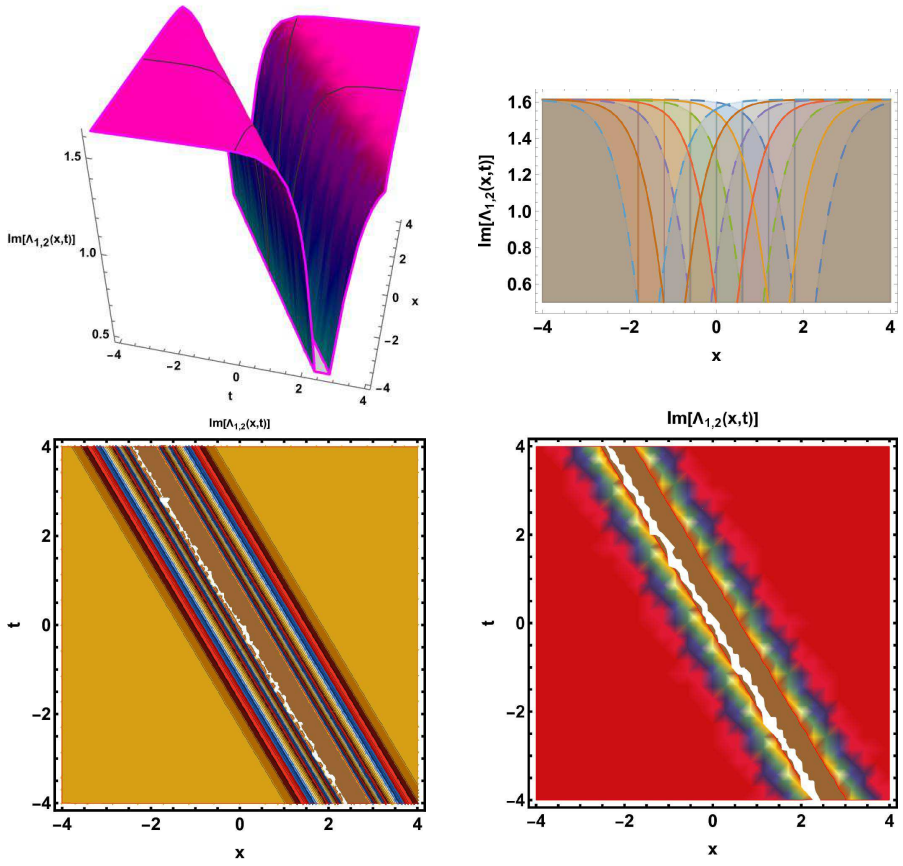


Fig. 13. Physical visualization of the singular-type solution of Eq. (72) for $q = -2.2$, $\wp_2 = -0.6$, $\wp_4 = 0.7$, $\wp_5 = 0.5$, $\alpha = 1$, $\beta = 0.4$, $\mu = 0.6$, and $m = 0.44$.

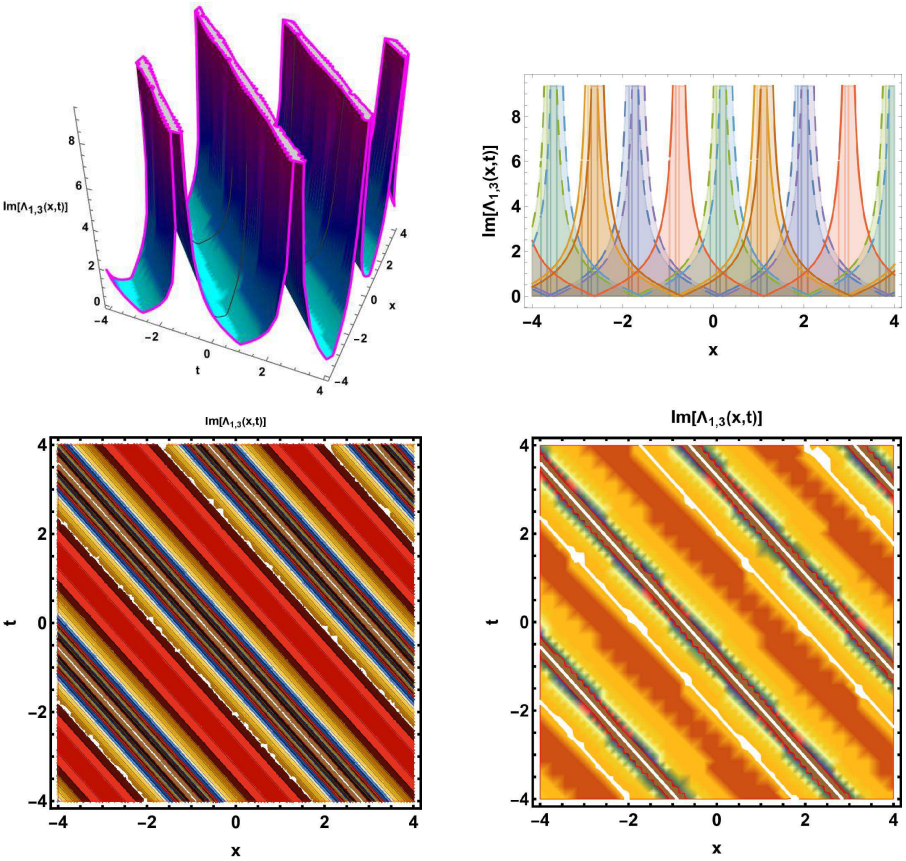


Fig. 14. Physical visualization of the periodic-type solution of Eq. (73) for $q = 0.9$, $\wp_2 = 0.7$, $\wp_4 = 2.62$, $\wp_5 = 1.5$, $\mu = 0.9$, $m = 0.7$, $\alpha = 1$, and $\beta = 0.49$.

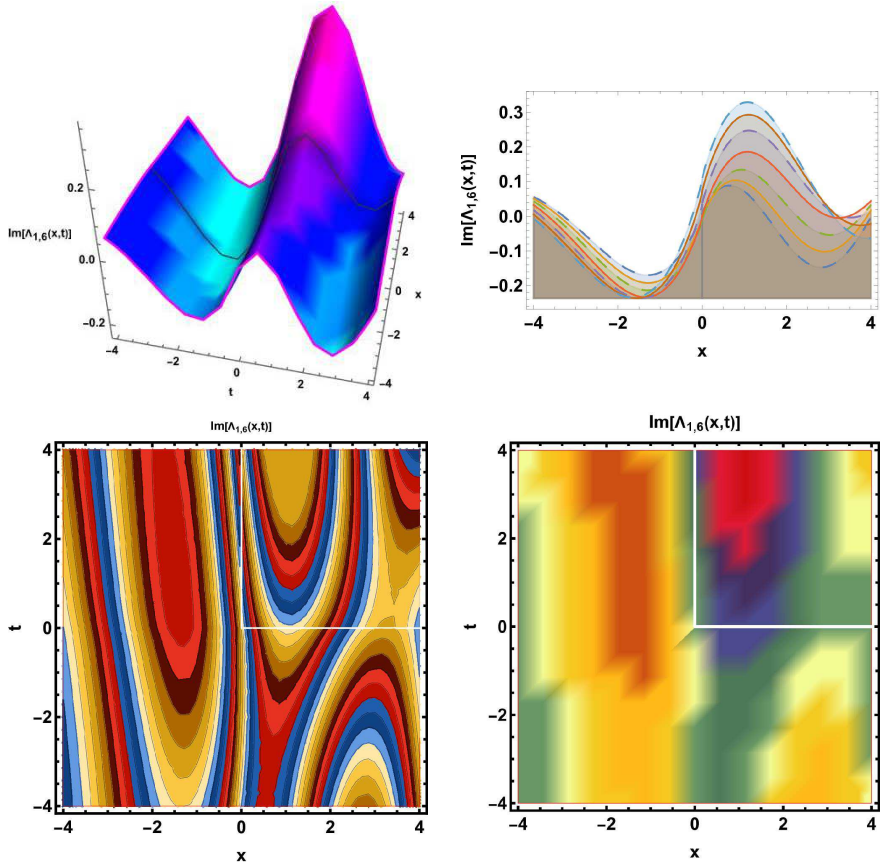


Fig. 15. Physical visualization of the dark-type solution of Eq. (77) for $q = -0.09$, $\lambda_0 = 0.66$, $\wp_2 = 0.1$, $\wp_4 = 0.7$, $\wp_5 = 0.5$, $\alpha = 0.89$, $\beta = 0.78$, $\mu = -0.55$, and $m = 0.44$.

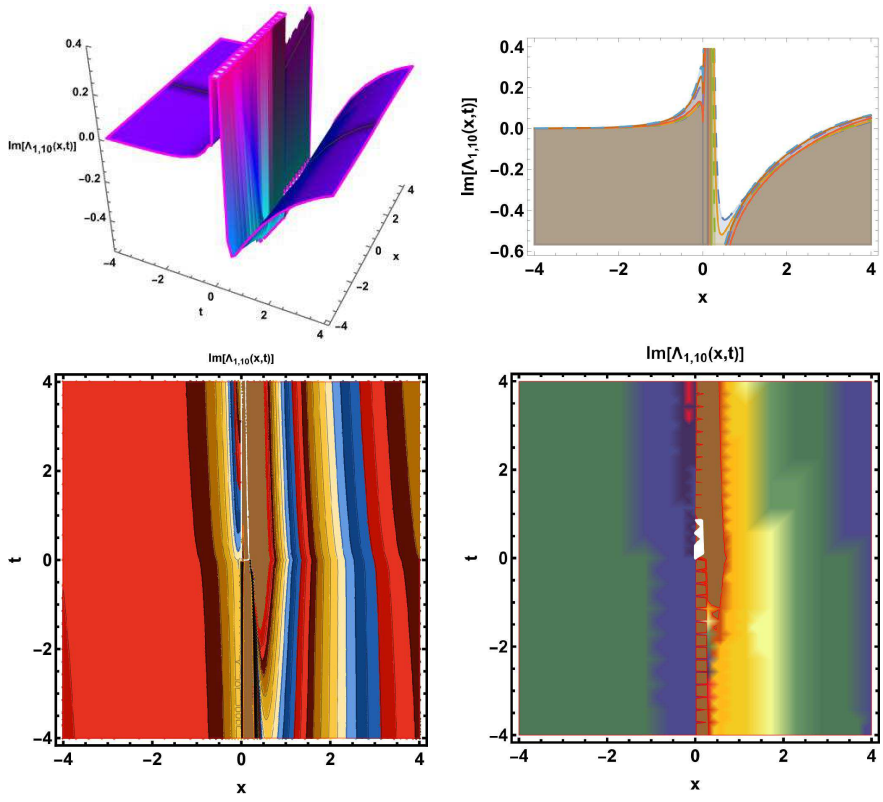


Fig. 16. Physical visualization of the rational-type wave structure obtained from Eq. (81) for $q = 0$, $\lambda_0 = 0.7$, $\wp_2 = 0.89$, $\wp_4 = 0.07$, $\wp_5 = 0.75$, $\alpha = 0.6$, $\beta = 0.78$, $\mu = 0.05$, and $m = 1.8$.

This classification highlights how the employed analytical methods collectively reveal diverse nonlinear optical wave dynamics within the FDENLSM framework.

7. Conclusion remarks

This study provides significant insights into the high-order FDENLSM through multifaceted analytical techniques, namely the MSSE method, the new Kudryashov approach, and the improved $\mathcal{F}$-expansion technique. We have obtained distinct forms of soliton W-shaped, bell-shaped, peakon, hyperbolic, and mixed trigonometric wave solutions. Furthermore, by employing the linear stability analysis method, the MI of the M-FDENLSM has been explored, and the MI gain has also been analyzed, demonstrating that the proposed model is stable. The primary contribution of this work is to demonstrate the versatility and efficacy of the aforementioned strategies in providing accurate solutions to the governing model. This study highlights the adaptability of the FDENLSM equation, which has practical applications in a number of domains, such as fluid dynamics and nonlinear optics. In the future, these analytical approaches can be extended to other higher-order nonlinear models incorporating stochastic noise effects, paving the way for more realistic and accurate representations of complex physical systems. Furthermore, examining parametric variations and their effects on the dynamics of the system can uncover more fascinating phenomena.

Acknowledgments

The authors extend their appreciation to the Deanship of Scientific Research and Libraries at Princess Nourah bint Abdulrahman University for funding this research work through the Research Group Project (Grant No. RG-2025- 08).

References

[1] Zhu X, Xia P, He Q, Ni Z and Ni L 2023 *Int. J. Bio-Inspired Comput.* **21** 106
[2] Akram S, Rahman M ur and Al-Essa L A 2025 *High Energy Density Phys.* **57** 101234
[3] Singh S, Sakkaravarthi K and Murugesan K 2023 *Chaos Solitons Fractals* **167** 113058
[4] Xing X, Han Y, Huang X, Chen W, Zhang Z, Liu M and Hu Q 2025 *Adv. Funct. Mater.* **35** e19204
[5] Xing X, Jiang Y, Huang X, Chen W, Wang K, Zhang Z and Liu M 2025 *Ultrafast Sci.* **5** 0115
[6] Cui X, Zhang Z, Liu M, Qi F and Liu W 2025 *Chin. Phys. Lett.* **42** 100402
[7] Rahman M ur, Akram S and Asif M 2025 *Sci. Rep.* **15** 34652
[8] Eskandari Z, Avazzadeh Z, Ghaziani R K and Li B 2025 *Math. Methods Appl. Sci.* **48** 7197
[9] Zhang X, Yang X and He Q 2022 *N. Am. J. Econ. Finance* **62** 101766
[10] Rahman M ur and Akram S 2026 *J. Appl. Anal. Comput.* **16** 1668
[11] Du W, He Q, Cao T and Wu J 2025 *Oper. Res. Lett.* **63** 107367
[12] Tsolias G A, Decker R J, Demirkaya A, Alexander T J, Parker R and Kevrekidis P G 2024 *Commun. Nonlinear Sci. Numer. Simul.* **125** 107362
[13] Li B, Zhang Y, Li X, Eskandari Z and He Q 2023 *J. Comput. Appl. Math.* **426** 115089
[14] Arshed S, Akram G, Sadaf M and Khan A 2023 *Opt. Quantum Electron.* **55** 922
[15] Akram S and Rahman M ur 2025 *Nonlinear Dyn.* **113** 32723
[16] Shakeel M, Shah N A and Chung J D 2023 *Ain Shams Eng. J.* **14** 101883
[17] Akram S, Saidani T and Rahman M ur 2025 *Math. Methods Appl. Sci.*
[18] Shagolshem S, Bira B and Nagaraja K V 2025 *Nonlinear Dyn.* **113** 11999
[19] Wang S 2023 *J. Opt.* **52** 1602
[20] Gulsen S, Hashemi M S, Alhefthi R, Inc M and Bicer H 2023 *J. Comput. Appl. Math.* **42** 221
[21] Yunus A O, Olayiwola M O, Omoloye M A and Oladapo A O 2023 *Healthcare Anal.* **3** 100167
[22] Yao S W, Gulsen S, Hashemi M S, Inc M and Bicer H 2023 *Results Phys.* **47** 106370
[23] Shen Y, Tian B, Zhou T Y and Gao X T 2023 *Nonlinear Dyn.* **111** 2641
[24] Ndoungalah S, Deffo G R, Djine A and Yamgoue S B 2023 *Chin. Phys. B* **32** 110505
[25] Ay N G and Yasar E 2023 *Pramana* **97** 106
[26] Zhang J R, Zhu F Y, Li W P and Shen Y J 2023 *Phys. Scr.* **98** 085217
[27] Akram S, Ahmad J, Sarwar S and Ali A 2023 *Opt. Quantum Electron.* **55** 450
[28] Shehata M S and Bekir A 2023 *Int. J. Mod. Phys. B* **37** 2350204
[29] Mathanaranjan T, Hashemi M S, Rezazadeh H, Akinyemi L and Bekir A 2023 *Commun. Theor. Phys.* **75** 085005
[30] Ali K K, Yusuf A, Alquran M and Tarla S 2023 *Commun. Theor. Phys.* **75** 085003
[31] Farooq K, Tedjani A H, Li Z and Hussain E 2025 *Fract. Fract.* **9** 436
[32] Ismael H F, Baskonus H M, Bulut H and Gao W 2023 *Opt. Quantum Electron.* **55** 303